Annual Reviews in Control 44 (2017) 211–225

Contents lists available at ScienceDirect

Annual Reviews in Control

journal homepage: www.elsevier.com/locate/arcontrol

Review article

Control of shallow waves of two unmixed fluids by backstepping

Mamadou Diagne[a], Shu-Xia Tang[b,*], Ababacar Diagne[c], Miroslav Krstic[b]

[a] Department of Mechanical, Aerospace, and Nuclear Engineering, Rensselaer Polytechnic Institute, Troy, NY 12180, USA
[b] Department of Mechanical and Aerospace Engineering, University of California, San Diego, La Jolla, CA 92093, USA
[c] Division of Scientific Computing, Department of Information Technology, Uppsala University, Box 337, Uppsala 75105, Sweden

ARTICLE INFO

Article history:
Received 10 February 2017
Revised 9 July 2017
Accepted 19 September 2017
Available online 18 October 2017

Keywords:
Shallow waves of unmixed fluids
Backstepping control
"Bi-layer" *Saint-Venant* model
Coupled hyperbolic PDEs

ABSTRACT

Among the existing global challenges, water system management is becoming more and more important as the consumption patterns are continually growing. The implication of water system regulation in irrigated agriculture and production of sustainable energy is self-evident nowadays. In the present paper, new perspectives are given on the control of water flowing in an open channel. Mathematically, these physical processes are described by coupled hyperbolic partial differential equations (PDEs). In view of the recent development in PDE control, backstepping methodology has been proven to be a powerful tool in the sense that it provides a systematic design technique. This paper presents the exponential stabilization results of two shallow wave systems including the shallow waves of two unmixed fluids.

Contents

1. Introduction

The management of water resource involves innumerable environmental and economic challenges of major concern, among which one can mention water management sustainability, intensively irrigated agriculture, flooding phenomena, production of renewable and sustainable energy through hydropower plants. Sev-

* Corresponding author.
E-mail addresses: diagnm@rpi.edu (M. Diagne), sht015@ucsd.edu (S.-X. Tang), babacar16@yahoo.fr (A. Diagne), krstic@ucsd.edu (M. Krstic).

https://doi.org/10.1016/j.arcontrol.2017.09.003
1367-5788/

eral efforts have been deployed during the last decades, to represent water management systems as dynamic systems that have the ability to predict consistently water resource evolution over time. From a cohesive perspective, water management systems are complexly integrated, some of which take into account the increasing demand of hydropower that has tremendous implications for the evolution of ecosystems (Winz, Brierley, & Trowsdale, 2009), and may even consist of conflicting sub-systems. For instance, to deal water-related problems that occurs in a complex network of open-channels consisting of

- nodes without storage capacity and nodes with storage capacity such as lakes and reservoirs with infiltration and evaporation,
- channels as river reaches as well as canals, ditches and inter-basin transfers,
- consumptive demands such as irrigated zones or municipal and industrial,

(Andreu, Capilla, & Sanchis 1996) developed a generalized decision-support system (DSS) for water-resources planning and operational management known as AQUATOOL.

The dynamics of open-channel hydraulic systems can be modeled by nonlinear coupled first-order PDEs, derived from the conservation of mass and momentum. For instance, estuaries (Horrevoets, Savenije, Schuurman, & Graas, 2004), rivers (Saint-Venant, 1871), irrigation canals (Malaterre, Rogers, & Schuurmans, 1998), overland flow (Tayfur, Kavvas, Govindaraju, & Storm, 1993; Wang, Chen, Boll, Stockle, & McCool, 2002), lake hydrodynamics (Zhao, Shen, Lai, & III, 1996) as well as coastal circulation (Bouchut, Fernández-Nieto, Mangeney, & Narbona-Reina, 2016; Broche, Salomon, Demaistre, & Devenon, 1986) are described by shallow water dynamic equations also called as *Saint-Venant* equations, neglecting the lateral movement of the water and assuming a constant velocity over the cross-section of an open channel.

The problematic of designing control tools to reinforce the regulation of the water level and the flow rate in open-channel hydraulic systems has a long history and is still driving the attention of researchers due to its challenging aspects. The controllers are usually actuated by adjusting the inflow and the outflow at the two boundaries of the channel. More precisely, changes in the volume of a canal pool connected to an upstream reservoir and a downstream reservoir occur when opening gates are actuated to vary the inflow and the outflow at the two channel boundaries.

Earlier attempts of controller designs consider the approximation of the linearized shallow water equations in the frequency domain as finite-dimensional systems in the spatial coordinate (Corriga, Fanni, Sanna, & Usai, 1982; Corriga, Salimbeni, Sanna, & Usai, 1988; Corriga, Sanna, & Usai, 1983; 1984; Schuurmans, Bosgra, & Brouwer, 1995; Shand, 1971). For example in Corriga et al. (1988), the solutions to the resulting set of ordinary differential equations are given by a distributed transfer matrix relating both the water depth and the water flow discharge at any point in the canal pool to upstream and downstream boundary discharges. Based on these solutions typically given in an analytical closed-loop form, some lumped parameter models equivalent to constant volume control models can then be constructed by accounting for the delay introduced by the wave propagation through two boundaries, enabling the design of simple linear state-feedback controllers. However, all these efforts are based on a non-realistic assumption that the system transfer matrices are uniform with respect to the spatial variable. Indeed, due to the intrinsically nonuniform transfer matrices, such methods are not actually enabling to reduce the complexity of the original control problem. Based on the method of characteristics, proportional boundary feedback controllers are successfully designed to cancel the oscillating modes induced by the reflection of propagating waves on the boundaries of the water pool (Litrico & Fromion, 2006).

Originating from an attempt to deal with a wave equation in Greenberg and Li (1984), more sophisticated controller designs for the shallow water systems are considered, which are based on stability analysis of the distributed parameter models (Coron, de Halleux, Bastin, & Novel, 2002; de Halleux & Bastin, 2002; de Halleux, Prieur, Coron, d'Andréa Novel, & Bastin, 2003; Prieur, Winkin, & Bastin, 2008; Santos & Prieur, 2008). Particularly in Santos and Prieur (2008), a boundary feedback controller is obtained through a direct analysis of the coupled nonlinear *Saint-Venant* equations subject to some perturbations such as frictions. The control performance has been tested successfully using the experimental data of the Sambre river, Belgium and an experimental test bed located in Valence, France. This control framework has then been generalized in Li (1994) for higher order systems.

A major improvement for the stabilization of shallow water equations has been driven by the application of Lyapunov-based control techniques to a one-dimensional *Saint-Venant* model. As stated in Coron, d'Andréa Novel, and Bastin (1999), for a segment, which is of irrigation channel described by *Saint-Venant* equations with two underflow gates at its boundaries, the total energy of the system is not a suitable Lyapunov candidate. Alternatively, the authors constructed an entropy-based Lyapunov function in this same paper, which achieved asymptotic stabilization of the shallow water equations with appropriate upstream and downstream boundary control actions. Since then, systematic Lyapunov-based techniques are used towards achieving efficient controlling of shallow water waves, i.e., the stabilization for coupled systems of one-dimensional hyperbolic PDEs through boundary controllers (Bastin & Coron, 2016). Later on, it was generalized to a "network of systems of conservation laws" in Bastin, Haut, Coron, and d'Andréa Novel (2007) and further improved in Coron, Novel, and Bastin (2007) for systems of conservation laws that can be diagonalized with Riemann Invariants with the introduction of a strict Lyapunov function by choosing properly the boundary control action (see also Tchousso, Besson, & Xu, 2009; Xu & Sallet, 2002 for a class of symmetric linear hyperbolic systems). As a result, Coron et al. (2007) achieved the regulation of the water level and flow in a horizontal open channel, and an extension of the design methodology allows the stabilization of sloping irrigation channels with an arbitrary number of cascading pools (Bastin, Coron, & d'Andréa Novel, 2009).

Various other methods have proven to be effective to ensure stability of such water driven fluvial processes. Some examples are, the proportional-integral boundary feedback controller presented in Santos, Bastin, Coron, and Novel (2008), Xu and Sallet (1999) and Bastin, Coron, and Tamasoiu (2015) (note that a generalization (Xu & Sallet, 1999) for linear hyperbolic systems can be found in Xu and Sallet (2014)), the infinite-dimensional linear matrix inequalities (LMI)-based design proposed in Diagne, Santos, and Rodrigues (2010) and Santos, Rodrigues, and Diagne (2008), and the proportional integral boundary feedback controller in Santos, Wu, and Rodrigues (2014).

Recently, a more complicated shallow water equation involving sediment dynamics has also been investigated. Such dynamics called as *Exner* equation represents the transport of the sediment in a water flow in the case where the sediment moves predominantly as bedload (Bastin & Coron, 2016, Page 25). Exponential stabilization is achieved for coupled linearized *Saint-Venant–Exner* models that are hyperbolic PDE systems by employing various methodologies such as a singular perturbation approach (Tang, Prieur, & Girard, 2014), explicit boundary dissipative conditions (Diagne, Bastin, & Coron, 2012), the ISS-Lyapunov function for time-varying hyperbolic systems (Prieur & Mazenc, 2012), and the backstepping technique (Diagne, Diagne, Tang, & Krstic, 2017). Among these approaches, backstepping is, to the best of our knowledge, the first one that could deal with supercritical flow regime without any restrictive conditions.

Backstepping boundary controller design methodology relies on the construction of an invertible transformation, generally called as backstepping transformation, which converts the original system into a stable target system. Therefore, induced by the exponential stability of the target system and continuity of the transformation and its inverse, exponential stability of the original system is guaranteed as well. For hyperbolic systems, the first application of the backstepping boundary control approach was introduced for the control of a 1D-wave PDE (Krstic, Guo, Balogh, & Smyshlyaev, 2008). The approach has been extended to 2×2 hyperbolic systems in Vazquez, Krstic, and Coron (2011) and lately generalized to linear hyperbolic systems with an arbitrary number of positive and one negative characteristic speed in Meglio, Vazquez, and Krstic (2013a). Recently, the problem of stabilizing general bidirectional systems of coupled hyperbolic PDEs has been solved in Hu, Meglio, Vazquez, and Krstic (2016) with backstepping technique. We also refer the readers to Coron, Vazquez, Krstic, and Bastin (2013) and its recent extension (Hu, Vazquez, Meglio, & Krstic, 2017), where quasi-linear hyperbolic systems are investigated. Moreover, for the class of general linear hyperbolic balance laws, a new proof on the optimal finite control time is presented in Coron, Hu, and Olive (2017), where the authors make use of the Fredholm backstepping transformation. Elsewhere, the problem of estimating state and boundary parameters in general heterodirectional linear hyperbolic systems have been recently studied in Anfinsen, Diagne, Aamo, and Krstic (2017). We refer the interested readers to Anfinsen and Aamo (2017), Auriol and Meglio (2016) and Deutscher (2017) for the research results of heterodirectional hyperbolic systems using boundary control.

The present paper demonstrates the feasibility of the backstepping design methodology for exponentially stabilizing shallow waves equations modeled by hyperbolic PDEs.

- First, the design procedure is introduced by studying the case of the *Saint-Venant–Exner* equation (Diagne et al., 2017) whose linearized and transformed version can be described by three coupled first-order hyperbolic PDEs, two of which have positive propagation speeds and one of which has a negative propagation speed. Here, the characteristic speeds are associated to the water and the sediment dynamics. In particular, supercritical flow regime, which are more difficult to deal with, can be stabilized by applying the general results of Meglio et al. (2013a).
- Second, the practical relevance of such a technique is further demonstrated through the stabilization of the "bi-layer"*Saint-Venant* equation, which is derived from the depth-averaged incompressible *Navier–Stokes* or *Euler* equations (Bouchut & Morales, 2008; Castro et al., 2004) and reflect the interfacial coupling phenomena that cannot be described by the *Saint-Venant* or *Exner* models. The "bi-layer" model describes the flow characteristic of two unmixed fluids, i.e., the superposition of two immiscible fluids with different densities and different flow rates. Some examples for these phenomena are, the flow involved in the Strait of Gibraltar where two layers of water with different properties are founded, and the denser Mediterranean and the Atlantic water (Castro, Garcia-Rodriguez, González-Vida, Macias, & Parés, 2007). Also, tsunamis generated by underwater landslide can be described by the "bi-layer" *Saint-Venant* model (Kim & Veque, 2008). Moreover, in some coastal regions (e.g., US Gulf Coast), the suppression of interfacial waves on dense fluid mud layers is needed to avoid a strong dissipation of surface waves, and the control of a "bi-layer" model can be useful to achieve this objective (Sheremet, Jaramillo, Su, Allison, & Holland, 2017). The PDE backstepping method is applied onto the feedback (exponential) stabilization problem of (a linear version of) the 1D "bi-layer" *Saint-Venant* model, which are quite relevant applications in fluid dynamics by exploiting the result in Hu et al. (2016). To the best of the authors' knowledge, this result is the first one on the stabilization of a shallow wave model of two unmixed fluids.

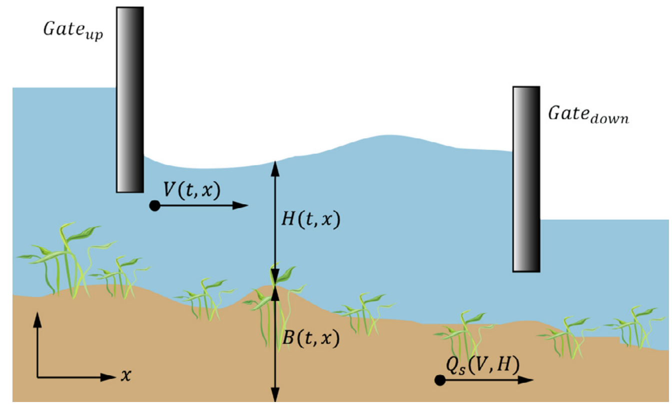

Fig. 1. A sketch of the channel.

The outline of this paper is as follows. In Section 2, we briefly recall the backstepping stabilization result of the 1D *Saint-Venant–Exner* model (Diagne et al., 2017) by presenting the key steps and providing some simulation results. In Section 3, the 1D "bi-layer" *Saint-Venant* model that governs the two unmixed fluids is first introduced based on its physical description. Then, a corresponding control problem related to its linearized version around a steady state is presented, based on which the backstepping controller designs are presented. Numerical simulations are provided in Section 4 for the linearized "bi-layer" *Saint-Venant* model as well, and this paper ends with a conclusion in Section 5.

2. Preliminary: backstepping control of a *Saint-Venant–Exner* model

In this section, the major steps for designing a backstepping controller for the linearized *Saint-Venant–Exner* equation are presented. Such a model describes the dynamics of water and sediment in a prismatic sloping open channel delimited by two gates. The control objective is to ensure (local) exponential stabilization of the water depth $H(t, x)$, the water velocity $V(t, x)$ and the bathymetry $B(t, x)$ which is the depth of the sediment layer above the channel bottom, to the desired setpoints by actuating the downstream gate (see Fig. 1).

2.1. *Physical description of the* Saint-Venant–Exner *model*

Given a pool of prismatic sloping open channel, the dynamics of the shallow water system is described by the coupling of *Saint-Venant* and *Exner* (SVE) equations (see e.g. Hudson & Sweby, 2003)

$$\frac{\partial H}{\partial t} + V\frac{\partial H}{\partial x} + H\frac{\partial V}{\partial x} = 0, \tag{1a}$$

$$\frac{\partial V}{\partial t} + V\frac{\partial V}{\partial x} + g\frac{\partial H}{\partial x} + g\frac{\partial B}{\partial x} = gS_b - C_f\frac{V^2}{H}, \tag{1b}$$

$$\frac{\partial B}{\partial t} + aV^2\frac{\partial V}{\partial x} = 0, \tag{1c}$$

where g is the gravity constant, S_b is the bottom slope of the channel, C_f is a friction coefficient and a is a parameter that encompasses the porosity and viscosity effects on the sediment dynamics. The coefficient a is defined as (cf Hudson & Sweby, 2003) $a = \frac{3A_g}{1-p_g}$, with p_g being the porosity parameter and A_g being the coefficient to control the interaction between the bed and the water flow. Indeed, this *Saint-Venant–Exner* model has been intensively studied in the existing literature. A significant amount of theoretical, numerical and experimental works dealing with the characteristics of water flow under movable bed can be found in Daly and Porporato (2017); Lanzoni, Siviglia, Frascati, and Seminara (2017) and the references therein. However, the boundary control of this system is left out in most of the contributions.

Linearization is the most frequently used method to consider the local behavior of nonlinear systems. In the few existing ones (Diagne et al., 2012; Diagne et al., 2017; Tang, Prieur et al., 2014) , a straightforward but lengthy computation that is performed on the linearized *Saint-Venant–Exner* model around a constant steady state $(H^*, V^*, B^*)^{\mathrm{T}}$ allows to express the system in Riemann coordinates as follows:

$$\frac{\partial \boldsymbol{\xi}}{\partial t} + \boldsymbol{\Lambda}\frac{\partial \boldsymbol{\xi}}{\partial x} - \boldsymbol{M}\boldsymbol{\xi} = 0, \tag{2}$$

$$\boldsymbol{\xi} = (\xi_1, \xi_2, \xi_3)^T, \quad \boldsymbol{\Lambda} = diag(\lambda_1, \lambda_2, \lambda_3), \tag{3}$$

$$\boldsymbol{M} = \begin{pmatrix} \alpha_1 & \alpha_2 & \alpha_3 \\ \alpha_1 & \alpha_2 & \alpha_3 \\ \alpha_1 & \alpha_2 & \alpha_3 \end{pmatrix}, \quad \alpha_k = \left(3V^* - 2\lambda_k\right) r_k, \tag{4}$$

where

$$r_k = C_f \frac{V^*}{H^*} \frac{\lambda_k}{(\lambda_k - \lambda_i)(\lambda_k - \lambda_j)},$$

and the characteristic coordinates are

$$\xi_k = \frac{H^*}{C_f V^* \lambda_k}\Big[\Big((V^* - \lambda_i)(V^* - \lambda_j) + gH^*\Big)(H(x,t) - H^*) + H^*\lambda_k(V(x,t) - V^*) + gH^*(B(x,t) - B^*)\Big]. \tag{5}$$

Here, λ_1, λ_3 are the characteristic velocities of the water flow and λ_2 is the characteristic velocity of the sediment motion. One should mention that the sediment motion is much slower than the water flow, physically. The flow characteristics depend on the Froude number $Fr = \frac{V^*}{\sqrt{gH^*}}$. According to Hudson and Sweby (2003), for a subcritical flow regime ($Fr < 1$), $\lambda_1 < 0 < \lambda_2 \ll \lambda_3$; and for a supercritical one ($Fr > 1$), $\lambda_2 < 0 < \lambda_1 < \lambda_3$.

2.2. Backstepping control problem formulation for the SVE model

For both the subcritical and supercritical regimes, the linear coupled PDE system (2)–(4) has two positive and one negative characteristic velocities and thus can be mapped into the following system through some coordinate transformations[1]:

$$\partial_t u_1 + \gamma_1 \partial_x u_1 = \sigma_{11} u_1 + \sigma_{12} u_2 + \alpha(x) w \tag{6a}$$

$$\partial_t u_2 + \gamma_2 \partial_x u_2 = \sigma_{21} u_1 + \sigma_{22} u_2 + \alpha(x) w \tag{6b}$$

$$\partial_t w - \mu \partial_x w = \theta_1(x) u_1 + \theta_2(x) u_2 \tag{6c}$$

[1] We refer the interested readers to Diagne et al. (2017) in which detailed derivations of the system (6) are presented. Also, Section 3 can be a good reference providing the derivation of a linearized coupled hyperbolic PDE system related to a more complex "bi-layer" *Saint-Venant* model.

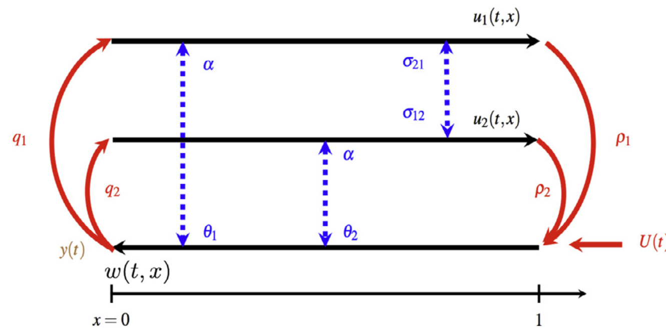

Fig. 2. Schematic of the hyperbolic system.

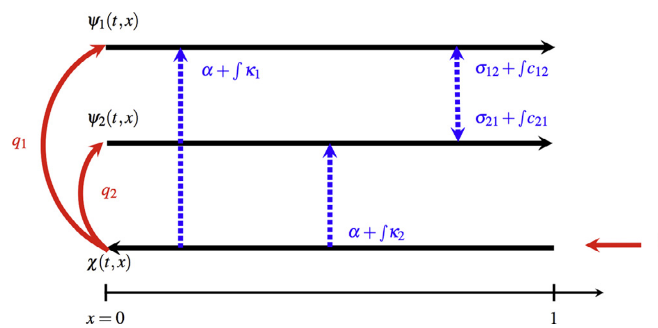

Fig. 3. Representation of the target system.

where the variables u_1, u_2, w are the distributed states and γ_1, γ_2, μ are positive constants.

For the system (6), the following boundary conditions are assumed, which can be considered as some special case of physical constraints:

$$u_i(t,0) = q_i w(t,0) \quad \text{for } i = 1, 2, \tag{7}$$

$$w(t,1) = \rho_1 u_1(t,1) + \rho_2 u_2(t,1) + U(t), \tag{8}$$

$$u_i(0,x) = u_i^0(x), \quad w(0,x) = w^0(x), \quad \text{for } i = 1, 2. \tag{9}$$

Here, $U(t)$ is the control input as shown in Figure 2 [2]

2.3. Backstepping control design

2.3.1. State feedback backstepping controller design

When designing a backstepping controller, the main difficulty is to find a suitable state transformation and a stable target system under the transformation. In order to stabilize the system (6)–(9) through backstepping, an invertible coordinate transformation (Diagne et al., 2017; Meglio et al., 2013b) is constructed as follows:

$$\psi_i(t,x) = u_i(t,x) \text{ for } i = 1,\ 2, \tag{10a}$$

$$\chi(t,x) = w(t,x) - \int_0^x k_1(x,\xi) u_1(t,\xi)\, d\xi - \int_0^x k_2(x,\xi) u_2(t,\xi)\, d\xi - \int_0^x k_3(x,\xi) w(t,\xi)\, d\xi \tag{10b}$$

aiming to convert the system (6)–(9) into the following target system:

[2] Figure 2and Figure 3are depicted in Meglio, Vazquez, and Krstic (2013b) for the general $n+1$ system.

$$\begin{aligned}\partial_t \psi_1 + \gamma_1 \partial_x \psi_1 = {} & \sigma_{11}\psi_1 + \sigma_{12}\psi_2 + \alpha(x)\chi \\ & + \int_0^x c_{11}(x,\xi)\psi_1(t,\xi)\,d\xi \\ & + \int_0^x c_{12}(x,\xi)\psi_2(t,\xi)\,d\xi \\ & + \int_0^x \kappa_1(x,\xi)\chi(t,\xi)\,d\xi, \end{aligned} \tag{11a}$$

$$\begin{aligned}\partial_t \psi_2 + \gamma_2 \partial_x \psi_2 = {} & \sigma_{21}\psi_1 + \sigma_{22}\psi_2 + \alpha(x)\chi \\ & + \int_0^x c_{21}(x,\xi)\psi_1(t,\xi)\,d\xi \\ & + \int_0^x c_{22}(x,\xi)\psi_2(t,\xi)\,d\xi \\ & + \int_0^x \kappa_2(x,\xi)\chi(t,\xi)\,d\xi, \end{aligned} \tag{11b}$$

$$\partial_t \chi - \mu \partial_x \chi = 0, \tag{11c}$$

$$\psi_i(t,0) = q_i \chi(t,0) \text{ for } i = 1,\, 2 \text{ and } \chi(t,1) = 0, \tag{11d}$$

where the kernel functions k_i, $i = 1,2,3$ of the transformation (10) and the functions $c_{ij}(\cdot)$, $\kappa_i(\cdot)$, $i = 1,2,\ j = 1,2$, are to be determined on the triangular domain $\mathbb{T} = \left\{(x,\xi) \in \mathbb{R}^2 \,|\, 0 \le \xi \le x \le 1\right\}$, to guarantee exponential stability of (11). One major difference between the original system (6) and the transformed system (11) is that the coupling in the negative propagating transport Eq. (6c) no longer appears in the new coordinate equations as shown in (11c). The dynamics of system (11) is schematically represented in Fig. 3.

Also, setting the boundary condition $\chi(t, 1)$ to zero in (11d) enables one to derive the following boundary feedback control law:

$$\begin{aligned} U(t) = {} & -\rho_1 u_1(t,1) - \rho_2 u_2(t,1) + \int_0^1 \Big[k_1(1,\xi)u_1(t,\xi) \\ & + k_2(1,\xi)u_2(t,\xi) + k_3(1,\xi)w(1,\xi)\Big]d\xi, \end{aligned} \tag{12}$$

where (8) and (10b) are used. From (12), one could notice that the implementation of the controller also requires the kernels k_i's to be known. Indeed, by comparing (6) and (11), such kernel functions need to satisfy the following first-order hyperbolic PDEs:

$$\begin{aligned}\mu\partial_x k_1(x,\xi) - \gamma_1 \partial_\xi k_1(x,\xi) = {} & \sigma_{11}k_1(x,\xi) + \sigma_{21}k_2(x,\xi) \\ & + \theta_1(\xi)k_3(x,\xi), \end{aligned} \tag{13a}$$

$$\begin{aligned}\mu\partial_x k_2(x,\xi) - \gamma_2 \partial_\xi k_2(x,\xi) = {} & \sigma_{12}k_1(x,\xi) + \sigma_{22}k_2(x,\xi) \\ & + \theta_2(\xi)k_3(x,\xi), \end{aligned} \tag{13b}$$

$$\mu\partial_x k_3(x,\xi) + \mu\partial_\xi k_3(x,\xi) = \alpha(\xi)k_1(x,\xi) + \alpha(\xi)k_2(x,\xi), \tag{13c}$$

$$k_1(x,x) = -\frac{\theta_1(x)}{\gamma_1 + \mu},\quad k_2(x,x) = -\frac{\theta_2(x)}{\gamma_2 + \mu}, \tag{13d}$$

$$\mu k_3(x,0) = q_1\gamma_1 k_1(x,0) + q_2\gamma_2 k_2(x,0). \tag{13e}$$

The existence, uniqueness, and continuity of the solutions to the system (13) are assessed by Theorem 5.3 in Meglio et al. (2013b). These kernels can be solved offline by simple finite element discretization on the domain $\mathbb{T}$. The transformation (10) is also proved to be invertible in Meglio et al. (2013b).

Furthermore, the coefficients κ_i's can be chosen to satisfy the following integral equation for $i = 1,\, 2$:

$$\kappa_i(x,\xi) = \alpha(x)k_3(x,\xi) + \int_\xi^x \kappa_i(x,s)k_3(s,\xi)\,ds. \tag{14}$$

Under the fact that the k_i's exist and are sufficiently smooth, the coefficients c_{ij}'s can be further chosen such that

$$c_{ij}(x,\xi) = \alpha(x)k_j(x,\xi) + \int_\xi^x \kappa_i(x,s)k_j(s,\xi)\,ds,\ i,\ j = 1,\ 2.$$

Then, the target system (11) can be proved to be exponentially stable by a Lyapunov function (Diagne et al., 2017; Meglio et al., 2013b)

$$V_1(t) = \int_0^1 \left[a_1 e^{-\delta_1 x}\left(\frac{\psi_1^2(t,x)}{\gamma_1} + \frac{\psi_2^2(t,x)}{\gamma_2}\right) + \frac{1+x}{\mu}\chi^2(t,x)\right]dx,$$

where a_1 and δ_1 are carefully chosen positive parameters.

Lemma 1. *(Diagne et al., 2017) For any given initial condition $(\psi_1^0,\ \psi_2^0,\ \chi^0)^T \in (\mathcal{L}^\in([\prime,\infty]))^3$ and under the assumption that $c_{ij},\ \kappa_i \in \mathcal{C}(\mathbb{T})$, the equilibrium $(\psi_1,\ \psi_2,\ \chi)^T = (0,\ 0,\ 0)^T$ of the target system (11) is $\mathcal{L}^\in$-exponentially stable.*

It is worth noting that an alternative proof can be provided for finite time stability by looking into the solution, as presented in Hu et al. (2016).

From the continuity and invertibility of the backstepping transformation (10), the equivalence between the original system (6) (with the control law (12)) and the target system (11) can be established.

Theorem 1. *Consider the system (6) and the control law (12). Under the assumptions that the initial data u_1^0, u_2^0, w^0 are in $(\mathcal{L}^\in([\prime,\infty]))^3$, the state $(u_1,\ u_2,\ w)^T$ is exponentially stable at the origin in the $\mathcal{L}^\in$ sense.*

2.3.2. Output feedback control design

The feedback controller (12) is implementable only in the case that a full state measurement across the spatial domain is available, however, the measurement of the distributed states is not doable in most flow control problems. Generally, boundary sensing approach, which is more feasible, is employed for control purposes. Next a state observer is designed in order to recover the state at each point of the whole spatial domain based on boundary measurements $y(t) = w(t, 0)$.

Part I: observer design. Denoting the estimated state as $(\hat{u}_1,\ \hat{u}_2,\ \hat{w})^T$, the following state estimator can be associated to system (6):

$$\begin{aligned}\partial_t \hat{u}_1 + \gamma_1 \partial_x \hat{u}_1 = {} & \sigma_{11}\hat{u}_1 + \sigma_{12}\hat{u}_2 + \alpha(x)\hat{w} \\ & - p_1(x)[y(t) - \hat{w}(t,0)], \end{aligned} \tag{15a}$$

$$\begin{aligned}\partial_t \hat{u}_2 + \gamma_2 \partial_x \hat{u}_2 = {} & \sigma_{21}\hat{u}_1 + \sigma_{22}\hat{u}_2 + \alpha(x)\hat{w} \\ & - p_2(x)[y(t) - \hat{w}(t,0)], \end{aligned} \tag{15b}$$

$$\begin{aligned}\partial_t \hat{w} - \mu \partial_x \hat{w} = {} & \theta_1(x)\hat{u}_1 + \theta_2(x)\hat{u}_2 \\ & - p_3(x)[y(t) - \hat{w}(t,0)], \end{aligned} \tag{15c}$$

$$\hat{u}_i(t,0) = q_i y(t) \quad \text{for } i = 1, 2, \tag{15d}$$

$$\hat{w}(t,1) = \rho_1 \hat{u}_1(t,1) + \rho_2 \hat{u}_2(t,1) + U(t). \tag{15e}$$

Looking into the structure of this observer, it consists of a copy of the original plant plus some observer error injection terms, where the injection gains $p_1(x)$, $p_2(x)$ and $p_3(x)$ need to be chosen such that the estimated state $(\hat{u}_1,\ \hat{u}_2,\ \hat{w})$ converges to the plant state (u_1, u_2, w) in some sense. In order for this to happen, the convergence of the observer error

$$\begin{pmatrix}\tilde{u}_1 & \tilde{u}_2 & \tilde{w}\end{pmatrix}^T = \begin{pmatrix}u_1-\hat{u}_1 & u_2-\hat{u}_2 & w-\hat{w}\end{pmatrix}^T, \tag{16}$$

must hold. In other words, the following error system

$$\partial_t\tilde{u}_1+\gamma_1\partial_x\tilde{u}_1 = \sigma_{11}\tilde{u}_1+\sigma_{12}\tilde{u}_2+\alpha(x)\tilde{w}+p_1(x)\tilde{w}(t,0), \tag{17a}$$

$$\partial_t\tilde{u}_2+\gamma_2\partial_x\tilde{u}_2 = \sigma_{21}\tilde{u}_1+\sigma_{22}\tilde{u}_2+\alpha(x)\tilde{w}+p_2(x)\tilde{w}(t,0), \tag{17b}$$

$$\partial_t\tilde{w}-\mu\partial_x\tilde{w} = \theta_1(x)\tilde{u}_1+\theta_2(x)\tilde{u}_2+p_3(x)\tilde{w}(t,0), \tag{17c}$$

$$\tilde{u}_i(t,0)=0 \quad \text{for } i=1,2, \tag{17d}$$

$$\tilde{w}(t,1)=\rho_1\tilde{u}_1(t,1)+\rho_2\tilde{u}_2(t,1) \tag{17e}$$

must converge to the origin for some careful choices of the gain functions $p_1(x)$, $p_2(x)$ and $p_3(x)$.

As in the previous section, the following backstepping transformation (Meglio et al., 2013b) is applied:

$$\tilde{u}_i(t,x)=\tilde{\pi}_i(t,x)+\int_0^x m_i(x,\xi)\tilde{\phi}(t,\xi)\,d\xi \quad i=1,2, \tag{18a}$$

$$\tilde{w}(t,x)=\tilde{\phi}(t,x)+\int_0^x m_3(x,\xi)\tilde{\phi}(t,\xi)\,d\xi, \tag{18b}$$

where the functions m_i, defined on the triangular domain $\mathbb{T}$, satisfy the following well-posed system:

$$\gamma_1\partial_x m_1-\mu\partial_\xi m_1=\sigma_{11}m_1+\sigma_{12}m_2+\alpha(x)m_3, \tag{19a}$$

$$\gamma_2\partial_x m_2-\mu\partial_\xi m_2=\sigma_{21}m_1+\sigma_{22}m_2+\alpha(x)m_3, \tag{19b}$$

$$\mu\partial_x m_3+\mu\partial_\xi m_3=-\theta_1(x)m_1-\theta_2(x)m_2, \tag{19c}$$

$$m_1(x,x)=\frac{1}{\gamma_1+\mu}\alpha(x),\ \ m_2(x,x)=\frac{1}{\gamma_2+\mu}\alpha(x), \tag{19d}$$

$$m_3(1,\xi)=\rho_1 m_1(1,\xi)+\rho_2 m_2(1,\xi). \tag{19e}$$

As a result, the error system (17) is mapped into the following system:

$$\partial_t\tilde{\pi}_1+\gamma_1\partial_x\tilde{\pi}_1=\sigma_{11}\tilde{\pi}_1+\sigma_{12}\tilde{\pi}_2+\int_0^x g_{11}(x,\xi)\tilde{\pi}_1(t,\xi)\,d\xi + \int_0^x g_{12}(x,\xi)\tilde{\pi}_2(t,\xi)\,d\xi, \tag{20a}$$

$$\partial_t\tilde{\pi}_2+\gamma_2\partial_x\tilde{\pi}_2=\sigma_{21}\tilde{\pi}_1+\sigma_{22}\tilde{\pi}_2+\int_0^x g_{21}(x,\xi)\tilde{\pi}_1(t,\xi)\,d\xi + \int_0^x g_{22}(x,\xi)\tilde{\pi}_2(t,\xi)\,d\xi, \tag{20b}$$

$$\partial_t\tilde{\phi}-\mu\partial_x\tilde{\phi}=\theta_1(x)\tilde{\pi}_1+\theta_2(x)\tilde{\pi}_2+\int_0^x h_1(x,\xi)\tilde{\pi}_1(t,\xi)\,d\xi + \int_0^x h_2(x,\xi)\tilde{\pi}_2(t,\xi)\,d\xi, \tag{20c}$$

with the boundary conditions as

$$\tilde{\pi}_i(t,0)=0,\ \tilde{\phi}(t,1)=\rho_1\tilde{\pi}_1(t,1)+\rho_2\tilde{\pi}_2(t,1), \tag{21}$$

for $i=1,\ 2,$ where the integral coupling coefficients are given by

$$h_i(x,\xi)=-\theta(\xi)m_3(x,\xi)-\int_\xi^x m_3(x,s)h_i(s,\xi)\,ds, \tag{22a}$$

$$g_{i,j}(x,\xi)=-\ \theta_j(\xi)m_i(x,\xi) - \int_\xi^x m_i(x,s)h_j(s,\xi)\,ds,\ \text{for } \{i,\ j\}=1,\ 2. \tag{22b}$$

Moreover, the observer gains are defined by

$$p_i(x)=\mu m_i(x,0) \text{ for } i=1,\ 2,\ 3. \tag{23}$$

Exponential stability holds for the system (20), which can be proved by the following Lyapunov function (Diagne et al., 2017; Meglio et al., 2013b):

$$V_2(t)=\int_0^1\left[a_2e^{-\delta_2 x}\left(\frac{\tilde{\pi}_1^2(t,x)}{\gamma_1}+\frac{\tilde{\pi}_2^2(t,x)}{\gamma_2}\right)+\frac{e^{\delta_2 x}}{\mu}\tilde{\phi}^2(t,x)\right]dx,$$

where a_2 and δ_2 are strictly positive parameters that are carefully determined.

Lemma 2. *Under the assumptions that the initial condition $\tilde{\pi}_1^0$, $\tilde{\pi}_2^0$, $\tilde{\phi}^0\in\mathcal{L}^\in([\prime,\infty])$ and the functions g_{ij}, $h_i\in\ \mathcal{C}(\mathbb{T})$, the system (20) with boundary conditions (21) and integral coupling coefficients (23) is exponentially stable in the $\mathcal{L}^\in$ sense.*

With the invertibility and continuity of the transformation (18), equivalence between the error system (17) and the target system (20) can be established. Thus, the following theorem holds.

Theorem 2. *Under the assumptions that the initial data are in $(\mathcal{L}^\in([\prime,\infty]))^3$, the observer system (15) (with the coefficient functions $p_i(x)$, $i=\overline{1,3}$ determined by (19) and (23)) exponentially converges to the system (6) in the $\mathcal{L}^\in$ sense.*

Part II: Output feedback backstepping controller design. Combining the controller (12), which requires a full state measurement, and the observer (15), which reconstructs the distributed state based on an output measurement $w(t,\,0)$, an observer-based output feedback controller can be designed.

Theorem 3. *Consider the $(u_1, u_2, w)^T$-system (6) together with the $\overline{(\hat{u}_1,\ \hat{u}_2,\ \hat{w})}^T$-observer (15) (with the coefficient functions $p_i(x)$, $i=\overline{1,3}$ determined by (19) and (23)). For a given initial condition $(u_1^0,\ u_2^0,\ w^0,\ \hat{u}_1^0,\ \hat{u}_2^0,\ \hat{w}^0)^T\in(\mathcal{L}^\in([\prime,\ \infty]))^6$ and the control law*

$$U(t)=-\rho_1u_1(t,1)-\rho_2u_2(t,1)+\int_0^1\Big[k_1(1,\xi)\hat{u}_1(t,\xi) + k_2(1,\xi)\hat{u}_2(t,\xi)+k_3(1,\xi)\hat{w}(1,\xi)\Big]d\xi, \tag{24}$$

where k_1, k_2 and k_3 satisfy (13), the $(u_1,\ u_2,\ w,\ \hat{u}_1,\ \hat{u}_2,\ \hat{w})^T$-system is exponentially stable in the sense of the $\mathcal{L}^\in$-norm.

The proof can be found in Krstic and Smyshlyaev (2008, Section 5.2) by constructing a weighted Lyapunov function.

2.4. *Simulation of the output feedback controller under a supercritical flow regime*

$T=10$, $\Delta x=0.01$, $p_g=0.02$, $C_f=0.15$, $\rho_2=1.5$, $q_1=q_2=1.5$.

In this subsection, the dynamic of the closed-loop system (6), together with the output feedback control law (24), is simulated. The parameters of the physical model together with the set point $(H^*,\ V^*,\ B^*)$ are listed in Table 1. Linearizing the system (1) around

Table 1
Parameters.

CFL	A_g	ρ_1	ρ_2	H^*	U^*	B^*
0.8	0.002	1	1.5	2	5	0.4

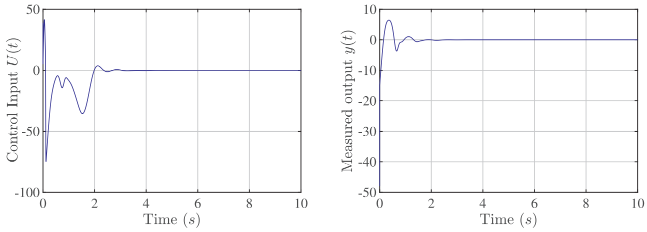

(a) Output control law (b) Measured output

Fig. 4. Evolution of the control law and the measured output.

the set point (H^*, V^*, B^*) gives the corresponding characteristic velocities $\lambda_1 = 1.87$, $\lambda_2 = -0.5$ and $\lambda_3 = 8.13$. A supercritical flow regime is considered setting the Froude number to $Fr = 1.13$. Physically, a high velocity profile and a low water level are considered to be the setpoint in this simulation.

The initial bottom topography is chosen as

$$B(0,x) = 0.4\left(1 + 0.25\exp\left(-\frac{(x-0.5)^2}{0.003}\right)\right),$$

which presents a Gaussian distribution centered at the middle of the domain. The initial water level and its velocity field are computed, respectively as

$$H(0,x) = 2.5 - B(0,x), \quad V(0,x) = \frac{10 sin(\pi x)}{H(0,x)}.$$

Using initial conditions of the physical system (1), namely, $H(0, x)$, $V(0, x)$ and $B(0, x)$, the initial data of the characteristic variables w, u_1 and u_2 are computed from (5).

In order to implement the control law (24), the kernel PDEs (13) are solved numerically offline and the values of the kernels k_1, k_2 and k_3 at $x = 1$ are employed. In sight of the triangular shape of the kernel function domain $\mathbb{T}$, an accurate finite volume scheme (a modified Roe scheme) can be employed to advance in time and space the hyperbolic evolutionary system (6). The solution to the kernel problem is computed accurately by using the quadratic finite element P_2. Moreover, the finite element setup is used to compute the kernel gain $p_i(x)$ defined in (23). Elsewhere, the computation of the control law (24) also requires the solution of the system (19), which is solved numerically on time and space using a finite element setup. Fig. 4 shows the evolution in time of the control input $U(t)$ at downstream, and the output measurement $y(t)$ at upstream. Clearly, the amplitude of $U(t)$ decreases in time and vanishes for $t \geq 4\,s$ as shown in Fig. 4(a) and the amplitude of the output measurement $y(t)$ decreases in time and tends to zero after $t \geq 3\,s$ as depicted in Fig. 4(b). The dynamics of the $\mathcal{L}^{\epsilon}$-norm are directly related to the magnitude of the propagation speeds λ_i (see. Fig. 5). Under this supercritical flow regime, it is remarkable that the backstepping output feedback control law (Fig. 5(a)) achieves exponential stability compared to the approach in Diagne et al. (2012) (Fig. 5(b)), which leads to an unstable dynamics. This striking fact is justified knowing that the conditions of Theorem 2 (cf Diagne et al., 2012) are not fulfilled in this specific case. Fig. 6 describes the space and time dynamics of the plant, and is consistent with the numerical results presented above. As time increases, it can be noticed that the perturbation in the overall system decreases and vanishes later.

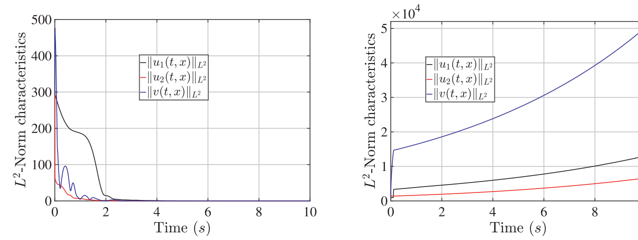

(a) Backstepping design. (b) Lyapunov design [34]

Fig. 5. Evolution of the norms of the characteristic solutions.

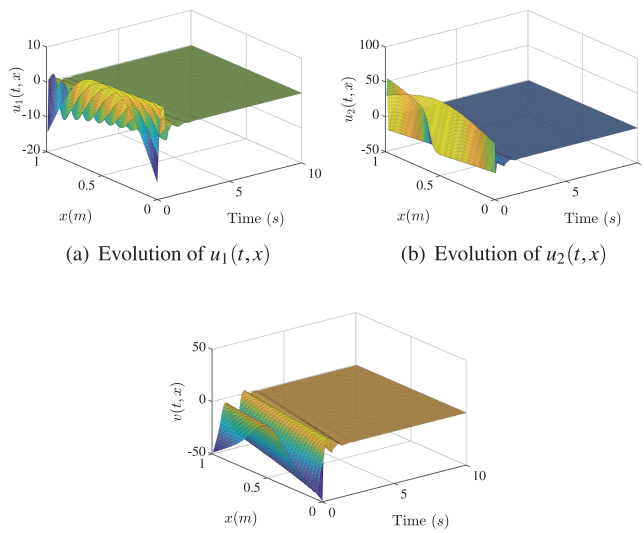

(a) Evolution of $u_1(t,x)$ (b) Evolution of $u_2(t,x)$

(c) Evolution of $v(t,x)$

Fig. 6. Behavior in time and space of the distributed states.

The presented numerical simulations of system (6) subject to the backstepping feedback control $U(t)$, is stabilized around the zero equilibrium as expected from the theoretical part.

The simulations verify the physical importance of the result in this section. More precisely, the backstepping controller offers the possibility to stabilize the moving bed dynamics under a rapidly varying water flow with a relatively small depth, with a single boundary actuation.

3. Backstepping control of a “bi-layer” *Saint-Venant* model

“Bi-layer” *Saint-Venant* models are often used to describe more complex interaction between the sediment and the water layers in river flows, for which the major characteristic of the physical phenomena cannot be described by the *Saint-Venant–Exner* model and thus requires to adopt the bi-layer model accounting for two unmixed fluids with the lower layer consisting of dense mixture of water and moving sediment. In this section, a “bi-layer” *Saint-Venant* model is presented for the purpose of controlling these waves with fast dynamics.

3.1. *Physical description of the “bi-layer”* Saint-Venant *model*

Fig. 7 depicts a “bi-layer” shallow water flow of two unmixed fluids delimited by two gates. The dynamics of these two superposed immiscible layers of shallow water fluids could be modeled by the following 1D “bi-layer” *Saint-Venant* model:

$$\frac{\partial H_1}{\partial t} + \frac{\partial (H_1 U_1)}{\partial x} = 0, \tag{25a}$$

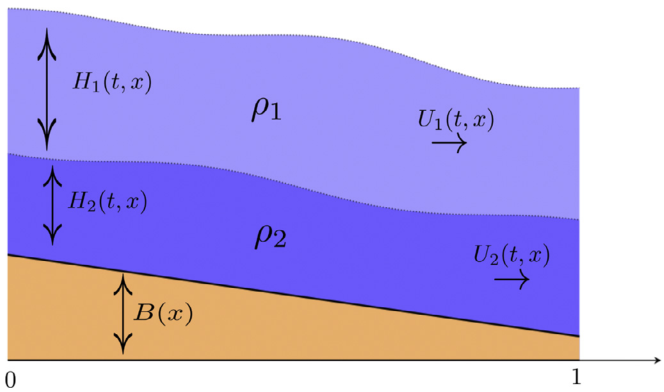

Fig. 7. “Bi-layer” shallow water flows.

$$\frac{\partial U_1}{\partial t}+U_1\frac{\partial U_1}{\partial x}+g\frac{\partial H_1}{\partial x}+g\frac{\partial H_2}{\partial x}+gS_b=S^f, \tag{25b}$$

$$\frac{\partial H_2}{\partial t}+\frac{\partial (H_2U_2)}{\partial x}=0, \tag{25c}$$

$$\frac{\partial U_2}{\partial t}+U_2\frac{\partial U_2}{\partial x}+g\frac{\partial H_2}{\partial x}+g\frac{\rho_1}{\rho_2}\frac{\partial H_1}{\partial x}+\frac{\rho_1}{\rho_2}gS_b=\frac{\rho_1}{\rho_2}S^f. \tag{25d}$$

In these equations, the indices 1 and 2 refer to the upper and lower layers, respectively, as depicted in Fig. 7 as well. The state variables H_i, U_i, $i=1,2$ represent respectively the thickness of the ith layer and the velocity. Each layer is assumed to have a constant density ρ_i, $i=1,2$ $(\rho_1<\rho_2)$. The system contains the source terms gS_b, and S^f, where S_b is the slope of the bathymetry and S^f stands for the friction between the two layers which is given by

$$S^f=\frac{C_f(U_1-U_2)^2}{H_1H_2}. \tag{26}$$

The equation (25) could be recast into the following form:

$$\frac{\partial W}{\partial t}+\frac{\partial F(W)}{\partial x}=S(W), \tag{27}$$

where $W:=\begin{bmatrix} H_1, & U_1, & H_2, & U_2\end{bmatrix}^T$ and the maps

$$F(W)=\begin{bmatrix} H_1U_1 \\ \frac{U_1^2}{2}+g(H_1+H_2) \\ H_2U_2 \\ \frac{U_2^2}{2}+g(H_2+rH_1)\end{bmatrix}, \tag{28}$$

$$S(W)=\begin{pmatrix}0 & S^f-gS_b & 0 & rS^f-rgS_b\end{pmatrix}^{\mathrm{T}}, \tag{29}$$

where $r=\rho_1/\rho_2$.

Physically, the ratio r characterizes the relative thickness of the bottom fluid layer with respect to the upper fluid layer. In the following parts of this section, we deal with the case when $r\ll 1$, namely, when the bottom fluid is much thicker than the upper fluid.

3.2. Linearization of the 1D “bi-layer” Saint-Venant model

Similar to the stabilization problem of the *Saint-Venant–Exner* equation, a local behavior of the nonlinear system (25) is considered around a steady state. denotes the corresponding Jacobian matrix function for (27). For the sake of simplification, we only consider here only the case when the steady state is constant, i.e., uniform in both time and space where $W^*=(H_1^*,U_1^*,H_2^*,U_2^*)^{\mathrm{T}}$ is the constant steady state associated with the system (27). One can note from (29) that the constant steady state is characterized by $S^f(W^*)=gS_b$. More precisely, from (26), the equilibrium set is chosen to match the following condition:

$$\frac{C_f(U_1^*-U_2^*)^2}{H_1^*H_2^*}=gS_b. \tag{30}$$

Defining the deviation of the state W with respect to the steady-state W^* as

$$w=W-W^*=[h_1,u_1,h_2,u_2]^T, \tag{31}$$

the linearized model of (27) is written as follows:

$$\partial_t w+A(W^*)\partial_x w=S_l(w), \tag{32}$$

where

$$A(W)=\begin{bmatrix} U_1 & H_1 & 0 & 0\\ g & U_1 & g & 0\\ 0 & 0 & U_2 & H_2\\ rg & 0 & g & U_2\end{bmatrix} \tag{33}$$

and

$$S_l(w)=[0,\ 1,\ 0,\ r]^{\mathrm{T}}\alpha_s^f(w) \tag{34}$$

with

$$\alpha_s^f=-a_1(h_1H_2^*+h_2H_1^*)+a_2(u_1-u_2), \tag{35}$$

$$a_1=C_f\left(\frac{U_1^*-U_2^*}{H_1^*H_2^*}\right)^2,\quad a_2=2C_f\frac{U_1^*-U_2^*}{H_1^*H_2^*}. \tag{36}$$

For the case of $r\approx 1$ and $U_1\approx U_2$, i.e., when the two-layers have very similar densities and flow rates, a first-order approximation of the eigenvalues is given in Nieto, Castro-Diaz, and Parés (2011) and Abgrall and Karni (2009).

The next step is to further simplify the problem by diagonalizing the system matrix $A(W^*)$ of (32) and expressing the system in Riemann coordinates. The characteristic equation derived from the matrix $A(W^*)$ is given by

$$\left((\lambda-U_1^*)^2-gH_1^*\right)\left((\lambda-U_2^*)^2-gH_2^*\right)=rg^2H_1^*H_2^*. \tag{37}$$

Following the results in Schijf and Schonfeld (1953), the eigenvalues of the system (32) in the case of $r\ll 1$ i.e., $\rho_1\ll\rho_2$ approach to those given as

$$\lambda_1=U_1^*-\sqrt{gH_1^*},\qquad \lambda_2=U_1^*+\sqrt{gH_1^*}, \tag{38a}$$

$$\lambda_3=U_2^*-\sqrt{gH_2^*},\qquad \lambda_4=U_2^*+\sqrt{gH_2^*}, \tag{38b}$$

which are the eigenvalues of $A(W^*)$ in the critical case of $r=0$. In what follows, the above λ_k $(k=\overline{1,4})$ are taken as the eigenvalues of $A(W^*)$. From (38), it is remarkable that the internal and external characteristics travel at different speeds. Indeed, the lower layer characteristics moves much slower than the upper ones. We consider the subcase when

$$\lambda_1,\lambda_3<0,\ \ \lambda_1\neq\lambda_3; \tag{39}$$

$$\lambda_2,\lambda_4>0,\ \ \lambda_2\neq\lambda_4, \tag{40}$$

which corresponds to a subcritical flow regime for each layer.

For a given eigenvalue λ_k $(k=\overline{1,4})$ of the matrix $A(W^*)$, the associated left eigenvector is expressed by

$$L_k^T w = -\left(\prod_{i\in\{1,2,3,4\}/\{k\}} (\lambda_i - \lambda_k)\right)^{-1} \times \begin{bmatrix} l_{k,1} & l_{k,2} & l_{k,3} & l_{k,4} \end{bmatrix}^{\mathrm{T}}, \tag{41}$$

where

$$l_{k,1} = U_1^{*3} - (\mathrm{tr}(A(W^*)) - \lambda_k)(U_1^{*2} + gH_1^*) + f_k + 3gH_1^* - \frac{\det(A(W^*))}{\lambda_k}, \tag{42}$$

$$l_{k,2} = 3H_1^*U_1^{*2} - 2H_1^*U_1^*(\mathrm{tr}(A(W^*)) - \lambda_k) + H_1^*(f_k + gH_1^*), \tag{43}$$

$$l_{k,3} = gH_1^*(7U_1^* - \lambda_k), \quad l_{k,4} = gH_1^*H_2^*. \tag{44}$$

The quantities f_k are defined by:

$$f_1 = (\lambda_3 + \lambda_2)\lambda_4 + \lambda_2\lambda_3,\ f_2 = (\lambda_3 + \lambda_1)\lambda_4 + \lambda_1\lambda_3, \tag{45}$$

$$f_3 = (\lambda_2 + \lambda_1)\lambda_4 + \lambda_1\lambda_2,\ f_4 = (\lambda_1 + \lambda_2)\lambda_3 + \lambda_1\lambda_2. \tag{46}$$

Multiplying w by L_k^{T} ($k = \overline{1,4}$), the following characteristic coordinate (Riemann invariant) is obtained:

$$\xi_k = L_k^T w = -\left(\prod_{i\in\{1,2,3,4\}/\{k\}} (\lambda_i - \lambda_k)\right)^{-1} \times \left[l_{k,1}h_1 + l_{k,2}u_1 + l_{k,3}h_2 + l_{k,4}u_2\right]. \tag{47}$$

Therefore, the variables w can be expressed in term of the Riemann invariant ξ as

$$w = \begin{pmatrix} 1 & 1 & 1 & 1 \\ \gamma_1 & \gamma_2 & \gamma_3 & \gamma_4 \\ \beta_1 & \beta_2 & \beta_3 & \beta_4 \\ \alpha_1 & \alpha_2 & \alpha_3 & \alpha_4 \end{pmatrix}\xi \tag{48}$$

where $\xi = \begin{pmatrix}\xi_1 & \xi_2 & \xi_3 & \xi_4\end{pmatrix}^{\mathrm{T}}$ and for $k = \overline{1,4}$,

$$\gamma_k = \frac{\lambda_k - 1}{H_1^*},\ \ \beta_k = \frac{1}{gH_1^*}\left(U_1^{*2} + 2(\lambda_k - 1)U_1^* - \lambda_k^2 + gH_1^*\right),$$

and

$$\alpha_k = \frac{1}{gH_1^*H_2^*}\Big((gH_1^*\beta_k - 2\lambda_k^2)U_2^* + 3U_1^{*3} + 7(\lambda_k - 1)U_1^{*2} + 2(gH_1^* - 2\lambda_k^2)U_1 + \lambda_k^2(\mathrm{tr}(A^*) - \lambda_k) + gH_1^*(\lambda_k + 2)\Big). \tag{49}$$

Let

$$\Lambda = \mathrm{diag}\{\lambda_1, \lambda_2, \lambda_3, \lambda_4\}, \tag{50}$$

then (32) can be rewritten as follows:

$$\partial_t\xi + \Lambda\partial_x\xi = M\xi, \tag{51}$$

where

$$M = [0,\ 1,\ 0,\ r]^{\mathrm{T}}\begin{pmatrix} a_2(\gamma_1 - \alpha_1) - a_1(H_2^* + \beta_1H_1^*) \\ a_2(\gamma_2 - \alpha_2) - a_1(H_2^* + \beta_2H_1^*) \\ a_2(\gamma_3 - \alpha_3) - a_1(H_2^* + \beta_3H_1^*) \\ a_2(\gamma_4 - \alpha_4) - a_1(H_2^* + \beta_4H_1^*) \end{pmatrix}^{\mathrm{T}}. \tag{52}$$

3.3. *Boundary control problem formulation for the "bi-layer"* Saint-Venant *model*

Define the state vectors as

$$u(t,x) = (\xi_2, \xi_4)^{\mathrm{T}},\ \ v(t,x) = (\xi_1, \xi_3)^{\mathrm{T}}$$

and introduce the transport speed matrices as

$$\Lambda^{\mathrm{r}} = \mathrm{diag}\{\lambda_1^{\mathrm{r}} = \lambda_2, \lambda_2^{\mathrm{r}} = \lambda_4\}, \tag{53}$$

$$\Lambda^{\mathrm{l}} = \mathrm{diag}\{\lambda_1^{\mathrm{l}} = -\lambda_1, \lambda_2^{\mathrm{l}} = -\lambda_3\}, \tag{54}$$

where it holds from (39)–(40) that

$$\lambda_1^{\mathrm{r}}, \lambda_2^{\mathrm{r}}, \lambda_1^{\mathrm{l}}, \lambda_2^{\mathrm{l}} > 0,\ \ \lambda_1^{\mathrm{r}} \neq \lambda_2^{\mathrm{r}},\ \ \lambda_1^{\mathrm{l}} \neq \lambda_2^{\mathrm{l}}. \tag{55}$$

Then, the system (51) is rewritten as

$$\partial_t u(t,x) + \Lambda^{\mathrm{r}}\partial_x u(t,x) = S^{\mathrm{r}}u(t,x) + S^{\mathrm{l}}v(t,x), \tag{56a}$$

$$\partial_t v(t,x) - \Lambda^{\mathrm{l}}\partial_x v(t,x) = 0, \tag{56b}$$

where the in-domain parameters are given as

$$S^{\mathrm{r}} = \begin{bmatrix} S_1 & S_2 \\ rS_1 & rS_2 \end{bmatrix},\ S^{\mathrm{l}} = \begin{bmatrix} S_3 & S_4 \\ rS_3 & rS_4 \end{bmatrix}, \tag{57}$$

where $S_i = a_2(\gamma_i - \alpha_i) - a_1(H_2^* + \beta_iH_1^*)$, $i = \overline{1,4}$. The objective is to stabilize the system (56) with the following boundary condition:

$$u(t,0) = Q_0v(t,0),\ \ v(t,1) = R_1u(t,1) + \mathcal{U}(t), \tag{58}$$

where the boundary parameters

$$Q_0 = \{q_{ij}\} \in \mathcal{M}_{2,2}(\mathbb{R}),\ \ R_1 = \{r_{ij}\} \in \mathcal{M}_{2,2}(\mathbb{R}), \tag{59}$$

and $\mathcal{U}(t) = [\mathcal{U}_1(t), \mathcal{U}_2(t)]^T$ consists of the boundary controllers we need to design.

3.4. *Backstepping control design*

3.4.1. *State feedback backstepping controller design*

The backstepping method could be used to design feedback boundary controllers for stabilizing the (linearized) "bi-layer" *Saint-Venant* system in Riemann invariants, i.e., (56)–(58), which consists of two leftwards and two rightwards propagating waves. In this section, the generalized backstepping methodology that enables the feedback stabilization of an arbitrary number of waves traveling in both directions (Diagne, Tang, Diagne, & Krstic, 2016a; 2016b; Hu et al., 2016) is applied to ensure the exponential stabilization of this linearized "bi-layer" model.

Part I: controller design. The following Volterra-type change of coordinates

$$\begin{pmatrix} \epsilon(t,x) \\ \beta(t,x) \end{pmatrix} = \begin{pmatrix} u(t,x) \\ v(t,x) \end{pmatrix} - \int_0^x \begin{pmatrix} 0 & 0 \\ G(x,\xi) & H(x,\xi) \end{pmatrix}\begin{pmatrix} u(t,\xi) \\ v(t,\xi) \end{pmatrix} d\xi \tag{60}$$

is performed to transform the system (56)–(58) into a finite-time stable target system Hu et al. (2016)

$$\partial_t\epsilon(t,x) + \Lambda^{\mathrm{r}}\partial_x\epsilon(t,x) = S^{\mathrm{r}}\epsilon(t,x) + S^{\mathrm{l}}\beta(t,x) + \int_0^x C^{\mathrm{r}}(x,\xi)\epsilon(t,\xi)d\xi + \int_0^x C^{\mathrm{l}}(x,\xi)\beta(t,\xi)d\xi, \tag{61a}$$

$$\partial_t\beta(t,x) - \Lambda^{\mathrm{l}}\partial_x\beta(t,x) = \Delta(x)\beta(0,t), \tag{61b}$$

$$\epsilon(t,0)=Q_0\beta(t,0), \tag{61c}$$

$$\beta(t,1)=0, \tag{61d}$$

where

$$\Delta(x)=\begin{bmatrix}0 & 0\\ \delta_{2,1}(x) & 0\end{bmatrix}, \tag{62}$$

and $C^{\mathrm{r}}, C^{\mathrm{l}}$ are matrices of functions defined on the triangular domain $\mathbb{T}$. Here, $C^{\mathrm{r}}, C^{\mathrm{l}}$ and $\delta_{2,1}(x)$ are all to be chosen.

Remark 1. Compared with the v-subsystem in the system (56)–(58) that the control is applied on and thus has a coupling term with the u-subsystem, the β-subsystem in the target system (61) has zero boundary input and is clearly finite-time stable. The remaining part, i.e., the target ϵ-subsystem, is then connected to the β-subsystem, making the resulting cascaded system finite-time stable.

In order to map the system (56)–(58) into the desired target system (61), the kernels G and H, defined on the domain $\mathbb{T}$, must satisfy the following system of equations:

$$\partial_\xi G(x,\xi)\Lambda^{\mathrm{r}}-\Lambda^{\mathrm{l}}\partial_x G(x,\xi)=-G(x,\xi)S^{\mathrm{r}}, \tag{63a}$$

$$\partial_\xi H(x,\xi)\Lambda^{\mathrm{r}}+\Lambda^{\mathrm{l}}\partial_x H(x,\xi)=G(x,\xi)S^{\mathrm{l}}, \tag{63b}$$

$$G(x,x)\Lambda^{\mathrm{r}}+\Lambda^{\mathrm{l}}G(x,x)=0, \tag{63c}$$

$$H(x,x)\Lambda^{\mathrm{l}}-\Lambda^{\mathrm{l}}H(x,x)=0, \tag{63d}$$

$$G(x,0)\Lambda^{\mathrm{r}}Q_0-H(x,0)\Lambda^{\mathrm{l}}=-\Delta(x). \tag{63e}$$

The existence and uniqueness of the backstepping transformation (60) could be guaranteed by adding some artificial boundary conditions (Hu et al., 2016). Also, as proved in Hu et al. (2016), the kernel PDE admit (61) admit a unique discontinuous which guarantees the existence of a unique inverse transformation. The inverse transformation is

$$\begin{pmatrix}u(t,x)\\ v(t,x)\end{pmatrix}=\begin{pmatrix}\epsilon(t,x)\\ \beta(t,x)\end{pmatrix}-\int_0^x\begin{pmatrix}0 & 0\\ \mathcal{G}(x,\xi) & \mathcal{H}(x,\xi)\end{pmatrix}\begin{pmatrix}\epsilon(t,\xi)\\ \beta(t,\xi)\end{pmatrix}d\xi, \tag{64}$$

where the kernels $\mathcal{G}(x,\xi), \mathcal{H}(x,\xi)$ satisfy

$$0=G(x,\xi)+\mathcal{G}(x,\xi)-\int_\xi^x\mathcal{H}(x,\eta)G(\eta,\xi)\,d\eta, \tag{65}$$

$$0=H(x,\xi)+\mathcal{H}(x,\xi)-\int_\xi^x\mathcal{H}(x,\eta)H(\eta,\xi)\,d\eta. \tag{66}$$

In the meantime, $\delta_{2,1}(x)$ and thus $\Delta(x)$ can be obtained. Also, the following equations are obtained for $C^{\mathrm{r}}(x,\xi), C^{\mathrm{l}}(x,\xi)$:

$$C^{\mathrm{r}}(x,\xi)=S^{\mathrm{l}}G(x,\xi)+\int_\xi^x C^{\mathrm{l}}(x,\eta)G(\xi,\eta)\,d\eta, \tag{67}$$

$$C^{\mathrm{l}}(x,\xi)=S^{\mathrm{l}}H(x,\xi)+\int_\xi^x C^{\mathrm{l}}(x,\eta)H(\xi,\eta)\,d\eta. \tag{68}$$

Hence, the control law $\mathcal{U}(t)$ can be obtained by plugging the transformation (60) into (58). Indeed, (61d) implies that

$$\mathcal{U}(t)=-R_1u(t,1)+\int_0^1[G(1,\xi)u(t,\xi)+H(1,\xi)v(t,\xi)]d\xi. \tag{69}$$

Part II: stability of the target system. In this part, the stability of the target system (61) is studied based on the Lyapunov method, which proves that it is exponentially stable as well.[3]

Assume there exist constants $M_0,\ M_1,\ \bar{q}>0$ such that

$$\|S^{\mathrm{r}}\|,\|S^{\mathrm{l}}\|\le M_0, \tag{70}$$

$$\|C^{\mathrm{r}}(x,\xi)\|,\|C^{\mathrm{l}}(x,\xi)\|\le M_1,\ \ \forall\xi\in[0,x],\forall x\in[0,1], \tag{71}$$

$$\|Q_0^TQ_0\|<\bar{q}, \tag{72}$$

where $\|\cdot\|$ stands for the 2-norm, and denote

$$\min\left\{\lambda_i^{\mathrm{r}},\lambda_i^{\mathrm{l}}\mid i=1,2\right\}:=\underline{\lambda}, \tag{73}$$

$$\max\left\{\lambda_i^{\mathrm{r}},\lambda_i^{\mathrm{l}}\mid i=1,2\right\}:=\overline{\lambda}. \tag{74}$$

The exponential stability of the target system (61)–(62) can be then proved.

Lemma 1. *For any given initial data $((\epsilon^0)^T,\ (\beta^0)^T)^T=(\epsilon^T(0,\cdot),\ \beta^T(0,\cdot))^T\in\left(\mathcal{L}^2([0,1])\right)^4$ and under the assumption that $C^{\mathrm{r}},\ C^{\mathrm{l}}\in\mathcal{C}(\mathbb{T})$, the equilibrium $(\epsilon^T,\ \beta^T)^T=(0,\ 0,\ 0,\ 0)^T$ of the target system (61)–(62) is exponentially stable in the $\mathcal{L}^2$-norm:*

$$\|(\epsilon^T(t,\cdot),\beta^T(t,\cdot))^T\|^2_{\mathcal{L}^2}:=\int_0^1\epsilon^T(t,x)\epsilon(t,x)+\beta^T(t,x)\beta(t,x)dx. \tag{75}$$

Proof. A Lyapunov function is constructed as follows:

$$\begin{aligned}V_3(t)&=\frac{1}{2}\int_0^1 e^{-\nu_1x}\epsilon^T(t,x)\mathbf{\Lambda}^{\mathrm{r}}_{\mathrm{inv}}\epsilon(t,x)dx\\&\quad+\frac{1}{2}\int_0^1(1+x)\beta^T(t,x)D\mathbf{\Lambda}^{\mathrm{l}}_{\mathrm{inv}}\beta(t,x)dx,\end{aligned} \tag{76}$$

where

$$\mathbf{\Lambda}^{\mathrm{r}}_{\mathrm{inv}}:=(\Lambda^{\mathrm{r}})^{-1}=\mathrm{diag}\left\{\frac{1}{\lambda_1^{\mathrm{r}}},\dots,\frac{1}{\lambda_n^{\mathrm{r}}}\right\}, \tag{77}$$

$$\mathbf{\Lambda}^{\mathrm{l}}_{\mathrm{inv}}:=\left(\Lambda^{\mathrm{l}}\right)^{-1}=\mathrm{diag}\left\{\frac{1}{\lambda_1^{\mathrm{l}}},\dots,\frac{1}{\lambda_m^{\mathrm{l}}}\right\}, \tag{78}$$

and $D=\mathrm{diag}\{d_1,\ d_2\}$. The constants ν_1 and d_1, d_2 are all positive parameters to be determined[4]. Then, we have

$$\begin{aligned}C_1\|(\epsilon^T(t,\cdot),\beta^T(t,\cdot))^T\|^2_{\mathcal{L}^2}&\le V_3(t)\\&\le C_2\|(\epsilon^T(t,\cdot),\beta^T(t,\cdot))^T\|^2_{\mathcal{L}^2},\end{aligned} \tag{79}$$

where the two positive constants are

$$C_1=\frac{1}{2\bar{\lambda}}\min\left\{e^{-\nu_1},\ d_1,\ d_2\right\}, \tag{80}$$

$$C_2=\frac{1}{2\underline{\lambda}}\max\{1,\ 2d_1,\ 2d_2\}. \tag{81}$$

[3] A different Lyapunov-based proof is also presented in Diagne, Tang, Diagne, and Krstic (2016b).

[4] A generalized version of the Lyapunov function was presented in Diagne et al. (2016a); 2016b) for dealing with the general class of coupled systems of $m+n$ heterodirectional transport PDEs, where the elements in the weighing matrix D are successively determined.

This ensures that $V_3(t)$ is positive definite.

Differentiating (76) with respect to time leads to

$$\dot{V}_3(t) = \int_0^1 e^{-\nu_1 x}\epsilon^T(t,x)\mathbf{\Lambda}_{\text{inv}}^{\text{r}}\partial_t\epsilon(t,x)dx + \int_0^1 (1+x)\beta^T(t,x)D\mathbf{\Lambda}_{\text{inv}}^{\text{r}}\partial_t\beta(t,x)dx. \quad (82)$$

Substituting equations (61a) and (61b) into (82), the following inequality is derived:

$$\begin{aligned}\dot{V}_3(t) =& \int_0^1 -e^{-\nu_1 x}\epsilon^T(t,x)\partial_x\epsilon(t,x)dx + \int_0^1 e^{-\nu_1 x}\epsilon^T(t,x)\mathbf{\Lambda}_{\text{inv}}^{\mathbf{r}}S^{\text{r}}\epsilon(t,x)dx \\ &+ \int_0^1 e^{-\nu_1 x}\epsilon^T(t,x)\mathbf{\Lambda}_{\text{inv}}^{\mathbf{r}}S^{\text{l}}\beta(t,x)dx \\ &+ \int_0^1 e^{-\nu_1 x}\epsilon^T(t,x)\left(\int_0^x \mathbf{\Lambda}_{\text{inv}}^{\mathbf{r}}C^{\text{r}}(x,\xi)\epsilon(\xi)d\xi\right)dx \\ &+ \int_0^1 e^{-\nu_1 x}\epsilon^T(t,x)\left(\int_0^x \mathbf{\Lambda}_{\text{inv}}^{\mathbf{r}}C^{\text{l}}(x,\xi)\beta(\xi)d\xi\right)dx \\ &+ \int_0^1 (1+x)\beta^T(t,x)D\partial_x\beta(t,x)dx + I(t), \end{aligned} \quad (83)$$

where

$$\begin{aligned} I(t) &= \int_0^1 (1+x)\beta^T(t,x)D\mathbf{\Lambda}_{\text{inv}}^{\mathbf{l}}\Delta(x)\beta(0,t)\,dx \\ &\leq \int_0^1 \frac{1+x}{2}\beta^T(t,x)\beta(t,x)\,dx \\ &\quad + \beta_1(t,0)^2\int_0^1 \frac{1+x}{2}d_2^2\frac{1}{(\lambda_2^{\text{l}})^2}\delta_{2,1}^2(x)dx. \end{aligned} \quad (84)$$

Further calculations give

$$\dot{V}_3(t) \leq J_1(t) + J_2(t), \quad (85)$$

where

$$\begin{aligned} J_1(t) =& \beta_1(t,0)^2\left\{\frac{\bar{q}}{2} - \frac{1}{2}d_1 + \int_0^1 \frac{1+x}{2}d_2^2\frac{1}{(\lambda_2^{\text{l}})^2}\delta_{2,1}^2(x)dx\right\} \\ &+ \beta_2(t,0)^2\left\{\frac{\bar{q}}{2} - \frac{1}{2}d_2\right\} \end{aligned} \quad (86)$$

and

$$\begin{aligned} J_2(t) =& -\frac{1}{2}f_1(\nu_1)\int_0^1 e^{-\nu_1 x}\epsilon^T(t,x)\epsilon(t,x)dx \\ &- \frac{1}{2}f_2(d_1,d_2,\nu_1)\int_0^1 \beta^T(t,x)\beta(t,x)\,dx \end{aligned} \quad (87)$$

with

$$f_1(\nu_1) = \nu_1 - 3\frac{M_0}{\underline{\lambda}} - \frac{M_1}{\underline{\lambda}}\left(2 + \frac{1}{\nu_1}\right), \quad (88)$$

$$f_2(d_1,d_2,\nu_1) = \min\{d_1,d_2\} - \frac{M_0}{\underline{\lambda}} - \frac{M_1}{\underline{\lambda}}\frac{1}{\nu_1}. \quad (89)$$

Choose the positive constants d_1, d_2 as follows:

$$d_2 \geq \bar{q}, \quad d_1 \geq \bar{q} + \int_0^1 (1+x)d_2^2\frac{1}{(\lambda_2^{\text{l}})^2}\delta_{2,1}^2(x)\,dx, \quad (90)$$

which guarantee that $J_1(t)$ is non-positive. Then, by choosing $\nu_1 > 0$ large enough to satisfy

$$f_1(\nu_1) > 0, \; f_3(\nu_1) := \bar{q} - \frac{M_0}{\underline{\lambda}} - \frac{M_1}{\underline{\lambda}}\frac{1}{\nu_1} > 0, \quad (91)$$

it holds that $f_2(\nu_1) \geq f_3(\nu_1) > 0$ and

$$\dot{V}_3(t) \leq J_2(t) \leq -c_1 V_3(t), \quad (92)$$

with

$$c_1 = \underline{\lambda}\min\left\{f_1(\nu_1), \; \frac{1}{\max\{d_1,d_2\}}f_2(d_1,d_2,\nu_1)\right\}, \quad (93)$$

which gives

$$V_3(t) \leq V_3(0)e^{-c_1 t}. \quad (94)$$

Finally, it can be derived from (79) that

$$\|(\epsilon^T(t,\cdot),\beta^T(t,\cdot))\|_{\mathcal{L}^2} \leq \sqrt{\frac{C_2}{C_1}}\|(\epsilon^0(\cdot),\beta^0(\cdot))\|_{\mathcal{L}^2}e^{-c_1 t}, \quad (95)$$

where C_1, C_2 are defined in (80) and (81). This completes the proof. □

Part III: stability of the closed-loop control system. The exponential stability of the target system (61), together with existence, uniqueness, regularity and invertibility of the backstepping transformation (60), guarantee the stability of the closed-loop control system (56)–(58) with the designed state feedback controller (69).

Theorem 4. *For any given initial data* $((u^0)^T, \; (v^0)^T)^T = (u^T(0,\cdot), \; v^T(0,\cdot))^T \in \left(\mathcal{L}^2([0,1])\right)^4$ *and under the assumption that* $C^{\text{r}}, \; C^{\text{l}} \in \mathcal{C}(\mathbb{T})$*, the equilibrium* $(u^T, \; v^T)^T = (0, \; 0, \; 0, \; 0)^T$ *of the closed-loop system (56)–(58) with controller (69) is exponentially stable in the sense of the norm* $\|(u^T(t,\cdot),v^T(t,\cdot))^T\|_{\mathcal{L}^2}^2$.

3.4.2. Output feedback backstepping controller design

As in the SVE case, the backstepping controller (69) requires a full state measurement across the spatial domain. In the situation when the only available data is the measured boundary output $y(t) = v(t,0)$, one needs to first construct an observer to recover the full state information of the system (56)–(58). Then, using these recovered data, an output feedback controller can be designed.

Part I: observer design. Next, a boundary state observer design is presented which helps avoid the full state measurement in a to-be-designed output feedback controller.

Defining the estimated state vector as $\left(\hat{u}^{\text{T}},\hat{v}^{\text{T}}\right)^{\text{T}}$, the following state observer consisting of a copy of the plant (56), (58) plus output injection terms:

$$\partial_t\hat{u} + \Lambda^{\text{r}}\partial_x\hat{u} = S^{\text{r}}\hat{u} + S^{\text{l}}\hat{v} - P_1(x)[y(t) - \hat{v}(t,0)], \quad (96a)$$

$$\partial_t\hat{v} - \Lambda^{\text{l}}\partial_x\hat{v} = -P_2(x)[y(t) - \hat{v}(t,0)], \quad (96b)$$

$$\hat{u}(t,0) = Q_0 y(t), \; \hat{v}(t,1) = R_1\hat{u}(t,1) + \mathcal{U}(t) \quad (96c)$$

is anticipated to achieve the reconstruction of the distributed state vector $(u^{\text{T}},v^{\text{T}})^{\text{T}}$.

Doing so, the vector $\begin{pmatrix}\tilde{u}^{\text{T}} & \tilde{v}^{\text{T}}\end{pmatrix}^{\text{T}} = \begin{pmatrix}u^{\text{T}} - \hat{u}^{\text{T}} & v^{\text{T}} - \hat{v}^{\text{T}}\end{pmatrix}^{\text{T}}$ is introduced which satisfies the following observer error system:

$$\partial_t\tilde{u} + \Lambda^{\text{r}}\partial_x\tilde{u} = S^{\text{r}}\tilde{u} + S^{\text{l}}\tilde{v} + P_1(x)\tilde{v}(t,0), \quad (97a)$$

$$\partial_t\tilde{v} - \Lambda^{\text{l}}\partial_x\tilde{v} = P_2(x)\tilde{v}(t,0), \quad (97b)$$

$$\tilde{u}(t,0) = 0, \; \tilde{v}(t,1) = R_1\tilde{u}(t,1). \quad (97c)$$

Thus, the objective is to determine the output injection coefficients $P_1(x)$ and $P_2(x)$ so that the observer error $(\tilde{u}^{\text{T}},\tilde{v}^{\text{T}})^{\text{T}}$ converges to the origin in the sense of the norm $\|(\tilde{u}^{\text{T}},\tilde{v}^{\text{T}})^{\text{T}}\|_{\mathcal{L}^2}$.

According to the backstepping control transformation (60), the following backstepping transformation inspired by the duality between controller and observer designs can be considered:

$$\begin{pmatrix}\tilde{u}(t,x)\\ \tilde{v}(t,x)\end{pmatrix} = \begin{pmatrix}\tilde{\epsilon}(t,x)\\ \tilde{\beta}(t,x)\end{pmatrix} + \int_0^x \begin{pmatrix}0 & M(x,\xi)\\ 0 & N(x,\xi)\end{pmatrix}\begin{pmatrix}\tilde{\epsilon}(t,\xi)\\ \tilde{\beta}(t,\xi)\end{pmatrix}d\xi, \quad (98)$$

where the to-be-determined kernels M and N are defined on the triangular domain $\mathbb{T}$ to map the error system (97) into the following exponentially stable target system:

$$\partial_t\tilde{\epsilon}+\Lambda^{\mathrm{r}}\partial_x\tilde{\epsilon}=S^{\mathrm{r}}\tilde{\epsilon}+\int_0^x D^{\mathrm{r}}(x,\xi)\tilde{\epsilon}(t,\xi)\,d\xi, \tag{99a}$$

$$\partial_t\tilde{\beta}-\Lambda^{\mathrm{l}}\partial_x\tilde{\beta}=\int_0^x D^{\mathrm{l}}(x,\xi)\tilde{\epsilon}(t,\xi)\,d\xi, \tag{99b}$$

$$\tilde{\epsilon}(t,0)=0,\ \ \tilde{\beta}(t,1)=R_1\tilde{\epsilon}(t,1)-\int_0^1\tilde{\Delta}(\xi)\tilde{\beta}(t,\xi)d\xi. \tag{99c}$$

Here, the functions $D^{\mathrm{r}}(x,\ \xi), D^{\mathrm{l}}(x,\ \xi)$ and $\tilde{\Delta}(\xi)$ are also to be determined.

By matching the error system (97) and the above target system, it can be derived that the transformation kernels $M(x,\ \xi)$ and $N(x,\ \xi)$ satisfy the following PDEs:

$$-M_\xi(x,\xi)\Lambda^{\mathrm{l}}+\Lambda^{\mathrm{r}}M_x(x,\xi)=S^{\mathrm{r}}M(x,\xi)+S^{\mathrm{l}}N(x,\xi), \tag{100a}$$

$$-N_\xi(x,\xi)\Lambda^{\mathrm{l}}-\Lambda^{\mathrm{l}}N_x(x,\xi)=0, \tag{100b}$$

$$M(x,x)\Lambda^{\mathrm{l}}+\Lambda^{\mathrm{r}}M(x,x)=S^{\mathrm{l}}, \tag{100c}$$

$$N(x,x)\Lambda^{\mathrm{l}}-\Lambda^{\mathrm{l}}N(x,x)=0, \tag{100d}$$

and meanwhile, the observer gains are given by

$$P_1(x)=-M(x,0)\Lambda^{\mathrm{l}},\ \ P_2(x)=N(x,0)\Lambda^{\mathrm{l}}. \tag{101}$$

Moreover, the functions $D^{\mathrm{r}}(x,\ \xi)$, $D^{\mathrm{l}}(x,\ \xi)$ and $\tilde{\Delta}(\xi)$ are defined by the following equations:

$$D^{\mathrm{r}}(x,\xi)+\int_\xi^x M(x,\eta)D^{\mathrm{l}}(\eta,\xi)d\eta=0, \tag{102}$$

$$D^{\mathrm{l}}(x,\xi)+\int_\xi^x N(x,\eta)D^{\mathrm{l}}(\eta,\xi)d\eta=0, \tag{103}$$

$$\tilde{\Delta}(\xi)=N(1,\xi)-R_1M(1,\xi). \tag{104}$$

The existence, uniqueness, and regularity of the transformation (98) are discussed in Hu et al. (2016), which guarantees the existence of a unique inverse transformation. The inverse transformation is

$$\begin{pmatrix}\tilde{\epsilon}(t,x)\\ \tilde{\beta}(t,x)\end{pmatrix}=\begin{pmatrix}\tilde{u}(t,x)\\ \tilde{v}(t,x)\end{pmatrix}+\int_0^x\begin{pmatrix}0 & \mathcal{M}(x,\xi)\\ 0 & \mathcal{N}(x,\xi)\end{pmatrix}\begin{pmatrix}\tilde{u}(t,x)\\ \tilde{v}(t,x)\end{pmatrix}d\xi, \tag{105}$$

and it can be derived from (98) and (105) that the kernels $\mathcal{M}(x,\xi),\mathcal{N}(x,\xi)$ need to satisfy

$$0=M(x,\xi)+\mathcal{M}(x,\xi)+\int_\xi^x\mathcal{M}(x,\eta)N(\eta,\xi)d\eta, \tag{106}$$

$$0=N(x,\xi)+\mathcal{N}(x,\xi)+\int_\xi^x\mathcal{N}(x,\eta)N(\eta,\xi)d\eta. \tag{107}$$

In order to solve the system of equations (106)–(107), the method of successive approximations can be used, see, Krstic and Smyshlyaev (2008, Section 4.4).

Assume there exists a constant $M_2>0$ such that

$$\|D^{\mathrm{r}}(x,\xi)\|,\ \|D^{\mathrm{l}}(x,\xi)\|,\ \|\tilde{\Delta}(\xi)\|\le M_2,\ \ \forall\xi\in[0,x],\ \ \forall x\in[0,1], \tag{108}$$

then exponential stability of the target system (99) can be proved.

Lemma 2. *For any given data $((\tilde{\epsilon}^0)^T,(\tilde{\beta}^0)^T)^T\in(\mathcal{L}^2([0,1]))^4$, the system (99), with (100), (102)–(104), is exponentially stable in the $\mathcal{L}^2$ sense. Furthermore, for any given data $((u^0)^T,\ (v^0)^T,\ (\hat{u}^0)^T,\ (\hat{v}^0)^T)^T\in(\mathcal{L}^2([0,1]))^8$, the observer (96) exponentially converges to the system (56) and (58) in the $\mathcal{L}^2$ sense.*

Proof. The following Lyapunov function is constructed:

$$V_4(t)=\frac{1}{2}d_3\int_0^1 e^{-\nu_2x}\tilde{\epsilon}^T(t,x)(\Lambda^{\mathrm{r}})^{-1}\tilde{\epsilon}(t,x)dx+\frac{1}{2}\int_0^1 e^{\nu_2x}\tilde{\beta}^T(t,x)(\Lambda^{\mathrm{l}})^{-1}\tilde{\beta}(t,x)dx, \tag{109}$$

where the constants d_3 and ν_2 are both positive parameters to be determined. In fact, V_4 is equivalent to the square of the state $\mathcal{L}^2$-norm:

$$C_3\|(\tilde{\epsilon}^T(t,\cdot),\tilde{\beta}^T(t,\cdot))^T\|_{\mathcal{L}^2}^2\le V_4(t)\ \le C_4\|(\tilde{\epsilon}^T(t,\cdot),\tilde{\beta}^T(t,\cdot))^T\|_{\mathcal{L}^2}^2, \tag{110}$$

where C_3, C_4 are two positive constants. Thus, the Lyapunov function $V_4(t)$ is positive definite.

Differentiating (109) with respect to time leads to

$$\dot{V}_4(t)=d_3\int_0^1 e^{-\nu_2x}\tilde{\epsilon}^T(t,x)(\Lambda^{\mathrm{r}})^{-1}\partial_t\tilde{\epsilon}(t,x)dx+\int_0^1 e^{\nu_2x}\tilde{\beta}^T(t,x)(\Lambda^{\mathrm{l}})^{-1}\partial_t\tilde{\beta}(t,x)dx. \tag{111}$$

Substituting the Eqs. (99a) and (99b) into (111), the following inequality is derived:

$$\begin{aligned}\dot{V}_4(t)\le&-\frac{1}{2}e^{-\nu_2}\tilde{\epsilon}^T(t,1)[d_3-4e^{\nu_2}R_1^TR_1]\tilde{\epsilon}(t,1)\\&-\frac{1}{2}f_4(d_3,\nu_2)\int_0^1 e^{-\nu_2x}\tilde{\epsilon}^T(t,x)\tilde{\epsilon}(t,x)dx\\&-\frac{1}{2}f_5(\nu_2)\int_0^1 e^{\nu_2x}\tilde{\beta}^T(t,x)\tilde{\beta}(t,x)\,dx,\end{aligned} \tag{112}$$

where

$$f_4(d_3,\nu_2)=\left(\nu_2-\frac{M_0+M_2}{\underline{\lambda}}\right)d_3-\frac{M_2}{\underline{\lambda}}\frac{1}{\nu_2}(1+e_2^{2\nu_2}-1), \tag{113}$$

$$f_5(\nu_2)=\nu_2-\frac{M_2}{\underline{\lambda}}-4M_2^2. \tag{114}$$

To ensure the exponential stability of the system (99), first, the positive parameter ν_2 is chosen as follows:

$$\nu_2>\max\left\{\frac{M_0+M_2}{\underline{\lambda}},\ \frac{M_2}{\underline{\lambda}}+4M_2^2\right\}, \tag{115}$$

and then the positive constant d_3 is chosen to satisfy

$$d_3\ge 4e^{\nu_2}R_1^TR_1,\ \ d_3>\frac{M_2(1+e_2^{2\nu_2}-1)}{\nu_2(\nu_2\underline{\lambda}-M_0-M_2)}. \tag{116}$$

With these choices of parameters, the positiveness of f_4, f_5 is guaranteed:

$$f_4(\nu_2,d_3)>0,\ \ f_5(\nu_2)>0, \tag{117}$$

and it holds that

$$\dot{V}_4(t) \leq -\frac{1}{2} f_4(d_3, \nu_2) \int_0^1 e^{-\nu_2 x} \tilde{\epsilon}^T(t,x) \tilde{\epsilon}(t,x) dx - \frac{1}{2} f_5(d_3, \nu_2) \int_0^1 e^{\nu_2 x} \tilde{\beta}^T(t,x) \tilde{\beta}(t,x)\, dx \leq -c_4 V_4(t), \tag{118}$$

for some positive constant c_4, which then gives

$$V_4(t) \leq V_4(0) e^{-c_4 t}. \tag{119}$$

Finally, it can be derived from (110) that

$$\|(\tilde{\epsilon}^T(t,\cdot), \tilde{\beta}^T(t,\cdot))\|_{\mathcal{L}^2} \leq \sqrt{\frac{C_4}{C_3}} \|(\tilde{\epsilon}^0(\cdot), \tilde{\beta}^0(\cdot))\|_{\mathcal{L}^2} e^{-c_2 t}. \tag{120}$$

This proves the exponential stability of the target error system (99), with (100) and (102)–(104). Then, from the continuity and invertibility of the backstepping transformation (98), exponential convergence of the designed observer (96) can be derived. □

Part II: Output feedback backstepping controller design. Based on the designed backstepping controller (69), which requires a full state measurement, and the observer (96), which reconstructs the state over the whole spatial domain through the boundary measurement $v(t, 0)$, an observer-based output feedback controller is designed:

$$\mathcal{U}(t) = -R_1 \hat{u}(t,1) + \int_0^1 [G(1,\xi)\hat{u}(t,\xi) + H(1,\xi)\hat{v}(t,\xi)] d\xi, \tag{121}$$

which works with the help of the observer (96).

Theorem 5. *For any given initial data $((u^0)^T, (v^0)^T, (\hat{u}^0)^T, (\hat{v}^0)^T)^T \in (\mathcal{L}^2([0,1]))^8$, the closed-loop $(u^T\ v^T,\ \hat{u}^T,\ \hat{v}^T)^T$-system, consisting of the original system (56)–(58), the observer (96) defined by (100) and (101), and the controller (121) with the kernels G and H defined by (61), is exponentially stable in the sense of the $\mathcal{L}^2$-norm:*

$$\|(u^T(t,\cdot), v^T(t,\cdot), \hat{u}^T(t,\cdot), \hat{v}^T(t,\cdot))\|^2_{\mathcal{L}^2} := \int_0^1 \Big[u^T(t,x)u(t,x) + v^T(t,x)v(t,x) + \hat{u}^T(t,x)\hat{u}(t,x) + \hat{v}^T(t,x)\hat{v}(t,x) \Big] dx.$$

The proof is omitted as well, for which a weighted Lyapunov function can be constructed by following the idea in Krstic and Smyshlyaev (2008, Section 5.2).

4. Simulation results

The goal of the following numerical simulations is to illustrate the efficiency of the designed output feedback controller $\mathcal{U}(t)$, namely, (121), to stabilize the linearized "bi-layer" *Saint-Venant* system in Riemann invariants (56)–(58) around the zero equilibrium.

The following data are considered as initial conditions for the layers 1 and 2 through the physical variables:

$$H_2(0,x) = 2 + 0.5 \exp\left(-\frac{(x-0.5)^2}{0.003} \right), \tag{122}$$

$$H_1(0,x) = 6 - H_2(x), \tag{123}$$

$$U_1(0,x) = \frac{10}{H_1(0,x)} + 3\sin(2\pi x), \tag{124}$$

$$U_2(0,x) = -\frac{10}{H_2(0,x)} - 3\sin(2\pi x). \tag{125}$$

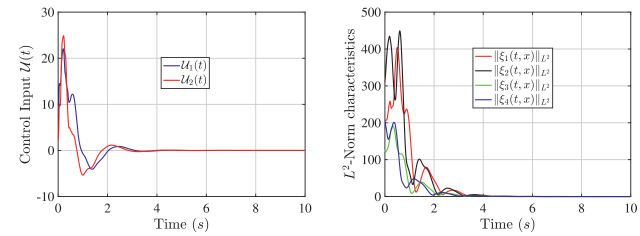

(a) control input (b) Characteristic solutions

Fig. 8. Evolution in time of the control input $U(t)$ and the norm of the characteristic solutions.

The initial data of the characteristic variables ξ_k, $(k = 1, 2, 3, 4)$ for the system (51) are computed as functions of the physical variables $H_i(0, x)$ and $U_i(0, x)$ for $i = 1, 2$, thanks to the relation (47).

The ratio r between the densities is set to 0.01 and the friction coefficient C_f is set to 0.05. The following uniform steady state: $H_1^* = 3$, $U_1^* = 1$, $H_2^* = 1$, $U_2^* = 0.95$ satisfies the constraints (30) with $S_b = \frac{1}{24000g}$. Moreover, with this choice of steady state, the characteristic speeds are given by: $\lambda_1 = -4.42$, $\lambda_2 = 6.42$, $\lambda_3 = -2.18$, $\lambda_4 = 4.08$. The ξ-solution is computed up to time $T = 10$s. Regarding the boundary conditions (58), it is assumed that

$$Q_0 = \begin{bmatrix} -1.5 & 0.01 \\ 0.01 & 1.5 \end{bmatrix}, \quad R_1 = \begin{bmatrix} 0.5 & 0.1 \\ 0.15 & -0.5 \end{bmatrix}. \tag{126}$$

As for the SVE simulation, a finite volume discretization method is performed for the evolution Eq. (51). The method uses a volume integral formulation of the problem with a finite partitioning set of volume to discretize, and it is well suited for discretizing computational fluid dynamics equations (Benkhaldoun & Seaid, 2010; Díaz, Chacón, Fernández-Nieto, & Parés, 2007; Veque, 2002). For instance, a general family of finite volume methods for non-homogeneous hyperbolic system is presented in Díaz et al. (2007) and some numerical tests to solve the "bi-layer" *Saint-Venant* model are provided.

Elsewhere, the computation of the control law requires the kernel values defined in (61). In sight of the triangular shape of the computational domain, we solve numerically the kernel system using the finite element method. Seen that the kernels are piecewise continuous, we adopt the discontinuous Galerkin (DG) finite element method to approximate the solution of the kernels. It is well-known in the literature that the DG technique yields accurate solution if at least piecewise quadratic polynomials are used for the basis function. The finite element method is particularly adapted for problems with complex geometries. An extensive review of these methods can be found in Thomee (2001).

In Fig. 8(a), the behavior in time of each component of the output feedback input controller is depicted. Despite the initial amplitudes, the second component of the control input $\mathcal{U}_2(t)$ decreases in time and vanishes, with the settling time being about 4s. The first component of the control input $\mathcal{U}_1(t)$ shows the same trend as well, with its amplitude decreasing in time and tending to zero, with the same settling time.

Fig. 8(b) depicts the evolution in time of the $\mathcal{L}^2$-norms of the characteristics for the output feedback closed-loop system. As expected from the theoretical part we observe clearly that the norm of the characteristics decreases in time and converges to zero. This shows that the closed-loop system (51) subjected to the output feedback controller converges to the zero equilibrium. Thereby, the "bi-layer" Saint-Venant model (25) converges to $(H_1^*, U_1^*, H_2^*, U_2^*)$.

Fig. 9 shows the evolution in time of the component of the solution to the closed-loop (51). The initial conditions are computed using the data in (122)–(125) and the considered uniform steady state. As expected from Fig. 8(b), it can be seen from Fig. 9 that

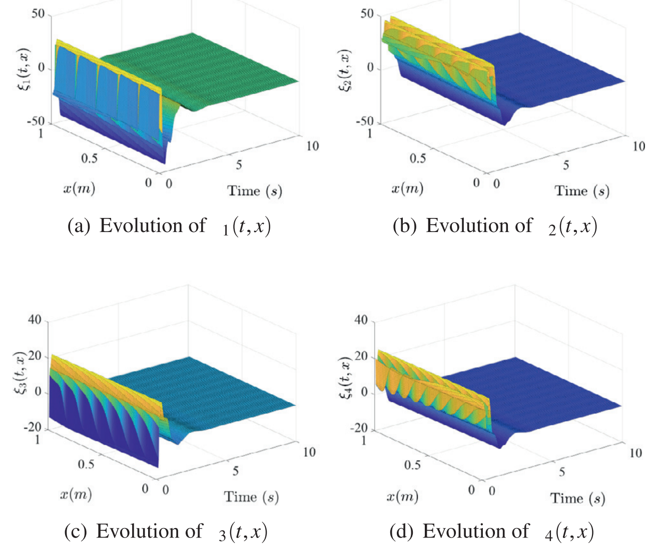

(a) Evolution of $_1(t,x)$ (b) Evolution of $_2(t,x)$

(c) Evolution of $_3(t,x)$ (d) Evolution of $_4(t,x)$

Fig. 9. Behavior in time and space of the distributed states.

each component of the ξ-solution converges to the origin and this is consistent with the theoretical results.

5. Conclusion and future works

This paper is devoted to the stabilization problem of shallow water waves that has been attracting the interest of control engineers for many decades. New perspectives are given based on some recent results that deal with exponential stabilization of linear coupled hyperbolic PDE systems. It has been proven that the backstepping methodology may unlock several important constraints regarding the design of boundary feedback control laws for such application.

The backstepping control of the linearized *Saint-Venant–Exner* model, which describes the dynamics of water and sediment in a prismatic sloping open channel delimited by two gates and can be transformed into a system that consists of two rightward and one leftward convecting transport PDEs, is first presented as a preliminary result. It is remarkable that a single boundary controller applied at the downstream gate enables the closed-loop feedback system to be exponentially regulated to a constant set point. No dissipativity restriction is imposed on the controller gain as in Diagne et al. (2012). Moreover, not only the subcritical but also the supercritical flow regimes can be treated by such a backstepping design.

Going to the depth of this contribution, the case of two unmixed fluids flowing in a portion of channel delimited by two gates is studied. Different from the SVE controller design, two backstepping controllers at the downstream gates are used to exponentially stabilize the corresponding "bi-layer" *Saint-Venant* model, which consists of two rightward and two leftward convecting transport PDEs.

It is worth mentioning that these two results stand among the first ones attempting to formulate and solve the control problems in the multi-layer flow dynamics. An effective control algorithm for boundary disturbance rejection (Tang, Guo, & Krstic, 2014; Tang & Krstic, 2014) can make a high impact on water system management. Also, extending the present results in the context of networks of open channel is an important but challenging future research direction.

Acknowledgment

The authors would like to thank Rafael Vazquez for suggesting the successive approximation method in the derivation of the inverse of the backstepping transformation in the observer design.

References

Abgrall, R., & Karni, S. (2009). Two-layer shallow water system: A relaxation approach. *SIAM Journal of Scientific Computing, 31*(3), 1603–1627.
Andreu, J., Capilla, J., & Sanchis, E. (1996). AQUATOOL, a generalized decision-support system for water-resources planning and operational management. *Journal of Hydrology, 177*(3), 269–291.
Anfinsen, H., & Aamo, O. M. (2017). Disturbance rejection in general heterodirectional 1d linear hyperbolic systems using collocated sensing and control. *Automatica, 76*, 230–242.
Anfinsen, H., Diagne, M., Aamo, O. M., & Krstic, M. (2017). Estimation of boundary parameters in general heterodirectional linear hyperbolic systems. *Automatica, 79*, 185–197.
Auriol, J., & Meglio, F. D. (2016). Minimum time control of heterodirectional linear coupled hyperbolic PDEs. *Automatica, 71*, 300–307.
Bastin, G., & Coron, J.-M. (2016). *Stability and boundary stabilization of 1-d hyperbolic systems*: 88. Birkhäuser.
Bastin, G., Coron, J.-M., & d'Andréa Novel, B. (2009). On Lyapunov stability of linearised Saint-Venant equations for a sloping channel. *Networks and Heterogeneous Media, 4*(2), 177–187.
Bastin, G., Coron, J.-M., & Tamasoiu, S. O. (2015). Stability of linear density-flow hyperbolic systems under PI boundary control. *Automatica, 53*, 37–42.
Bastin, G., Haut, B., Coron, J.-M., & d'Andréa Novel, B. (2007). Lyapunov stability analysis of networks of scalar conservation laws. *Networks and Heterogeneous Media, 2*(4), 749–757.
Benkhaldoun, F., & Seaid, M. (2010). A simple finite volume method for the shallow water equations. *Journal of Computational and Applied Mathematics, 234*(1), 58–72.
Bouchut, F., Fernández-Nieto, E. D., Mangeney, A., & Narbona-Reina, G. (2016). A two-phase two-layer model for fluidized granular flows with dilatancy effects 801. 166–221.
Bouchut, F., & Morales, d. L. T. (2008). An entropy satisfying scheme for two-layer shallow water equations with uncoupled treatment. *ESAIM: Mathematical Modelling and Numerical Analysis, 42*, 683–698.
Broche, P., Salomon, J., Demaistre, J., & Devenon, J. (1986). Tidal currents in baie de seine: Comparison of numerical modelling and high-frequency radar measurements. *Estuarine, Coastal and Shelf Science, 23*(4), 465–476.
Castro, J. M., Garcıa-Rodrıguez, J. A., González-Vida, J. M., Macıas, J., Parés, C., & Vázquez-Cendón, M. E. (2004). Numerical simulation of two-layer shallow water flows through channels with irregular geometry. *Journal of Computational Physics, 195*(1), 202–235.
Castro, M. J., Garcia-Rodriguez, J. A., González-Vida, J. M., Macias, J., & Parés, C. (2007). Improved FVM for two-layer shallow-water models: Application to the strait of gibraltar. *Advances in Engineering Software, 38*(6), 386–398.
Coron, J.-M., de Halleux, J., Bastin, G., & Novel, B. d. (2002). On boundary control design for quasi-linear hyperbolic systems with entropies as lyapunov functions. In *Proc. 41st IEEE conference on decision control, Las Vegas, NV* (pp. 3010–3014).
Coron, J.-M., Hu, L., & Olive, G. (2017). Finite-time boundary stabilization of general linear hyperbolic balance laws via fredholm backstepping transformation. arXiv: 1701.05067.
Coron, J.-M., d'Andréa Novel, B., & Bastin, G. (1999). A Lyapunov approach to control irrigation canals modeled by Saint–Venant equations. In *European control conference (ECC), karlsruhe* (pp. 3178–3183).
Coron, J.-M., Novel, B. d., & Bastin, G. (2007). A strict lyapunov function for boundary control of hyperbolic systems of conservation laws. *IEEE Transaction on Automatic Control, 52*(1), 2–11.
Coron, J.-M., Vazquez, R., Krstic, M., & Bastin, G. (2013). Local exponential H^2 stabilization of a 2×2 quasilinear hyperbolic system using backstepping. *SIAM Journal on Control and Optimization, 51*(3), 2005–2035.
Corriga, G., Fanni, A., Sanna, S., & Usai, G. (1982). A constant-volume control method for open channel operation. *International Journal of Modelling and Simulation, 2*(2), 108–112.
Corriga, G., Salimbeni, D., Sanna, S., & Usai, G. (1988). A control method for speeding up response of hydroelectric station power canals. *Applied Mathematical Modelling, 12*(6), 627–633.
Corriga, G., Sanna, S., & Usai, G. (1983). Sub-optimal constant-volume control for open channel networks. *Applied Mathematical Modelling, 7*(4), 262–267.
Corriga, G., Sanna, S., & Usai, G. (1984). Centralized control of irrigation canal systems. In *Channels and channel control structures, springer* (pp. 659–673).
Daly, E., & Porporato, A. (2017). Some self-similar solutions in river morphodynamics. *Water Resources Research, 41*(12).
Deutscher, J. (2017). Finite-time output regulation for linear 2×2 hyperbolic systems using backstepping. Automatica, 75, C, 54–62.
Diagne, A., Bastin, G., & Coron, J.-M. (2012). Lyapunov exponential stability of 1-d linear hyperbolic systems of balance laws. *Automatica, 48*(1), 109–114.
Diagne, A., Diagne, M., Tang, S.-X., & Krstic, M. (2017). Backstepping stabilization of the linearized *Saint–Venant–Exner* model. *Automatica, 76*, 345–354.

Diagne, A., Tang, S.-X., Diagne, M., & Krstic, M. (2016a). Output feedback stabilization of the bilayer Saint-Venant model. *ASME dynamic systems and control conference*.
Diagne, A., Tang, S.-X., Diagne, M., & Krstic, M. (2016b). State feedback stabilization of the linearized bilayer saint-venant model. *IFAC-PapersOnLine, 49*(8), 130–135.
Diagne, M., Santos, V. D., & Rodrigues, M. (2010). Une approche multi-modèles des équations de saint-venant : Une analyse de la stabilité par techniques LMI. In *Proceedings of sixième conférence internationale francophone d'automatique*. Nancy (France): CIFA.
Díaz, M. J. C., Chacón, T., Fernández-Nieto, E. D., & Parés, C. (2007). On well-balanced finite volume methods for non conservative non-homogeneous hyperbolic systems. *SIAM Journalon Scientific Computing, 29*(3), 1093–1126.
Greenberg, J. M., & Li, T. (1984). The effect of boundary damping for the quasilinear wave equation. *Journal of Differential Equations, 52*(1), 66–75. doi:10.1016/0022-0396(84)90135-9.
de Halleux, J., & Bastin, G. (2002). Stabilization of saint-venant equations using riemann invariants: Application to waterways with mobile spillways. *IFAC Proceedings, 35*(1), 131–136.
de Halleux, J., Prieur, C., Coron, J.-M., d'Andréa Novel, B., & Bastin, G. (2003). Boundary feedback control in networks of open-channels. Automatica, 39, 1365–1376.
Horrevoets, A., Savenije, H., Schuurman, J., & Graas, S. (2004). The influence of river discharge on tidal damping in alluvial estuaries. *Journal of Hydrology, 294*(4), 213–228.
Hu, L., Meglio, F. D., Vazquez, R., & Krstic, M. (2016). Control of homodirectional and general heterodirectional linear coupled hyperbolic PDEs. *IEEE Transactions on Automatic Control, 61*(11), 3301–3314.
Hu, L., Vazquez, R., Meglio, F. D., & Krstic, M. (2017). Boundary exponential stabilization of 1-d inhomogeneous quasilinear hyperbolic systems. arXiv:1512.03539.
Hudson, J., & Sweby, P. (2003). Formulations for numerically approximating hyperbolic systems governing sediment transport. *Journal of Scientific Computing, 19*, 225–252.
Kim, J., & Veque, R. J. L. (2008). Two-layer shallow water system and its applications. In *Proceedings of the twelth international conference on hyperbolic problems, maryland*.
Krstic, M., Guo, B. Z., Balogh, A., & Smyshlyaev, A. (2008). Output-feedback stabilization of an unstable wave equation. *Automatica, 44*(1), 63–74.
Krstic, M., & Smyshlyaev, A. (2008). Boundary control of PDEs: A course on backstepping designs. *SIAM, 16*.
Lanzoni, S., Siviglia, A., Frascati, A., & Seminara, G. (2017). Long waves in erodible channels and morphodynamic influence. *Water Resources Research, 42*(6).
Li, T.-T. (1994). Global classical solutions for quasi-linear hyperbolic systems. *Research in applied mathematics, masson and wiley*.
Litrico, X., & Fromion, V. (2006). Boundary control of linearized saint-venant equations oscillating modes. *Automatica, 42*(6), 967–972.
Malaterre, P. o., Rogers, D. C., & Schuurmans, J. (1998). Classification of canal control algorithms. *Journal of Irrigation and Drainage Engineering, 124*(1), 3–10.
Meglio, F. D., Vazquez, R., & Krstic, M. (2013a). Stabilization of a system of coupled first-order hyperbolic linear pdes with a single boundary input. *IEEE Transactions on Automatic Control, 58*(12), 3097–3111.
Meglio, F. D., Vazquez, R., & Krstic, M. (2013b). Stabilization of a system of coupled first-order hyperbolic linear PDEs with a single boundary input. *IEEE Transactions on Automatic Control, 58*(12), 3097–3111.
Nieto, E. F., Castro-Diaz, M. J., & Parés, C. (2011). On an intermediate field capturing riemann solver based on a parabolic viscosity matrix for the two-layer shallow water system. *Journal of Scientific Computing, 48*(1–3), 117–140.
Prieur, C., & Mazenc, F. (2012). ISS-Lyapunov functions for time-varying hyperbolic systems of balance laws. *Mathematics of Control, Signals, and Systems, 24*(1–2), 111–134.
Prieur, C., Winkin, J., & Bastin, G. (2008). Robust boundary control of systems of conservation laws. *Mathematics of Control Signals Systems, 20*(2), 173–197.
Saint-Venant, B. d. (1871). Theory of unsteady water flow, with application to river floods and to propagation of tides in river channels. *French Academy of Science, 73*(1871), 237–240.
Santos, V. D., Bastin, G., Coron, J. M., & Novel, B. d. (2008). Boundary control with integral action for hyperbolic systems of conservation laws: Stability and experiments. *Automatica, 44*(5), 1310–1318.
Santos, V. D., & Prieur, C. (2008). Boundary control of open channels with numerical and experimental validations. In *IEEE transactions on control systems technology: vol. 16* (pp. 1252–1264).
Santos, V. D., Rodrigues, M., & Diagne, M. (2008). A multi-models approach of Saint–Venants equations : A stability study by LMI. *International Journal of Applied Mathematics and Computer Science, 22*(3), 539–550.
Santos, V. D., Wu, Y., & Rodrigues, M. (2014). Design of a proportional integral control using operator theory for infinite dimensional hyperbolic systems. *IEEE Transactions on Control Systems Technology, 22*(5), 2024–2030.
Schijf, J., & Schonfeld, J. (1953). Theoretical considerations on the motion of salt and fresh water. In *Proc. of the minn. int. hydraulics conv. joint meeting IAHR and hyd. div. ASCE.* (pp. 321–333).
Schuurmans, J., Bosgra, O., & Brouwer, R. (1995). Open-channel flow model approximation for controller design. *Applied Mathematical Modelling, 19*(9), 525–530.
Shand, M. J. (1971). *Automatic downstream control systems for irrigation canals*. University of California: Hydraulic Engineering Laboratory.
Sheremet, A., Jaramillo, S., Su, S.-F., Allison, M., & Holland, K. (2017). Wave-mud interaction over the muddy atchafalaya subaqueous clinoform, louisiana, united states: Wave processes. *Journal of Geophysical Research: Oceans, 116*(C6).
Tang, S. X., Guo, B.-Z., & Krstic, M. (2014). Active disturbance rejection control for 2×2 hyperbolic systems with an input disturbance. In *IFAC world congress* (pp. 11385–11390).
Tang, S. X., & Krstic, M. (2014). Sliding mode control to the stabilization of a linear a $2\times\ 2$ hyperbolic system with boundary input disturbance. In *American control conference (ACC), IEEE* (pp. 1027–1032).
Tang, Y., Prieur, C., & Girard, A. (2014). Boundary control synthesis for hyperbolic systems: Asingular perturbation approach. *IEEE conference on decision and control,Los Angeles, California, USA*.
Tayfur, G., Kavvas, M. L., Govindaraju, R. S., & Storm, D. E. (1993). Applicability of st. venant equations for two-dimensional overland flows over rough infiltrating surfaces. *Journal of Hydraulic Engineering, 119*(1), 51–63.
Tchousso, A., Besson, T., & Xu, C.-Z. (2009). Exponential stability of distributed parameter systems governed by symmetric hyperbolic partial differential equations using lyapunov's second method. *ESAIM Control Optimisationand Calculusof Variations, 15*(2), 403–425.
Thomee, V. (2001). From finite differences to finite elements: A short history of numerical analysis of partial differential equations. *Journal of Computational and Applied Mathematics, 128*(1), 1–54.
Vazquez, R., Krstic, M., & Coron, J.-M. (2011). Backstepping boundary stabilization and state estimation of a $2\times\ 2$ linear hyperbolic system. In *2011 50th IEEE conference on decision and control and European control conference, IEEE* (pp. 4937–4942).
Veque, R. J. L. (2002). *Finite-volume methods for hyperbolic problems*. Cambridge University Press.
Wang, G.-T., Chen, S., Boll, J., Stockle, C., & McCool, D. (2002). Modelling overland flow based on Saint–Venant equations for a discretized hillslope system. *Hydrological Processes, 16*(12), 2409–2421.
Winz, I., Brierley, G., & Trowsdale, S. (2009). The use of system dynamics simulation in water resources management. *Water Resources Management, 23*(7), 1301–1323.
Xu, C., & Sallet, G. (1999). Proportional and integral regulation of irrigation canal systems governed by the Saint–Venant equation. In *Proceedings of the 14th world control congress, Beijing, China*.
Xu, C., & Sallet, G. (2002). Exponential stability and transfer functions of processes governed by symmetric hyperbolic systems. *ESAIM Control Optimisation and Calculus of Variations, 7*, 421–442.
Xu, C.-Z., & Sallet, G. (2014). Multivariable boundary pi control and regulation of a fluid flow system. *Mathematical Control and Related Fields, 4*(4), 501–520.
Zhao, D., Shen, H., Lai, J., & III, G. T. (1996). Approximate riemann solvers in fvm for 2d hydraulic shock wave modeling. *Journal of Hydraulic Engineering, 122*(12), 692–702.